

Random Projection Forests

Tyler M. Tomita¹, James Browne², Cencheng Shen³, Jesse L. Patsolic¹, Jason Yim⁴,
Carey E. Priebe¹, Randal Burns², Mauro Maggioni⁵, and Joshua T. Vogelstein¹

¹Center for Imaging Science, Johns Hopkins University, Baltimore, MD

²Department of Computer Science, Johns Hopkins University, Baltimore, MD

³Department of Applied Economics and Statistics, University of Delaware, Newark, DE

⁴DeepMind, London, UK

⁵Department of Mathematics, Johns Hopkins University, Baltimore, MD

Ensemble methods—particularly those based on decision trees—have recently demonstrated superior performance in a variety of machine learning settings. We introduce a generalization of many existing decision tree methods called “Random Projection Forests” (RPF), which is any decision forest that uses (possibly data dependent and random) linear projections. Using this framework, we introduce a special case, called “Lumberjack”, using very sparse random projections, that is, linear combinations of a small subset of features. Lumberjack obtains statistically significantly improved accuracy over Random Forests, Gradient Boosted Trees, and other approaches on a standard benchmark suites for classification with varying dimension, sample size, and number of classes. To illustrate how, why, and when Lumberjack outperforms other methods, we conduct extensive simulated experiments, in vectors, images, and nonlinear manifolds. Lumberjack typically yields improved performance over existing decision trees ensembles, while mitigating computational efficiency and scalability, and maintaining interpretability. Lumberjack can easily be incorporated into other ensemble methods such as boosting to obtain potentially similar gains.

1 Introduction

Over the last two decades, ensemble methods have risen to prominence as the state-of-the-art for general-purpose machine learning tasks. One of the most popular and consistently strong ensemble methods, which uses decision trees as the base learners, is Random Forests (RFs) [Fernandez-Delgado *et al.*, 2014; Caruana *et al.*, 2008; Caruana and Niculescu-Mizil, 2006]. More recently, another tree ensemble method known as gradient boosted decision trees (GBTs) has seen a spike in popularity, largely due to the release of a fast and scalable cross-platform implementation, XGBoost [Chen, 2018]. GBTs have been a key component of many Kaggle competition winning solutions as well as the winning solution of the Netflix prize [Chen and Guestrin, 2016].

RFs and XGBoost are ensembles of “axis-aligned” decision trees. With such decision trees, the feature space is recursively split along directions parallel to the coordinate axes. Thus, in cases in which the classes seem inseparable along any single dimension, RF requires very deep trees with complicated decision boundaries, leading to increased variance and over-fitting. To address this, Breiman also proposed and characterized Forest-RC (F-RC), which uses linear combinations of coordinates rather than individual coordinates, to split along. Since then, numerous other “oblique” decision forest methods have been proposed, including “Random Rotation Random Forest” (RR-RF) [Blaser and Fryzlewicz, 2016], and canonical correlation forests

(CCF) Rainforth and Wood [2015]. Unfortunately, these methods lose many of the desirable properties that RFs possess, such as speed, insensitivity to a large proportion of irrelevant inputs or noise, and interpretability. Furthermore, these oblique methods are often tested only on a fairly restricted set of real-world data sets.

We propose a method for learning an ensemble of decision trees called Random Projection Forests (RPF). The key insight behind RPF is that essentially all previously proposed ensemble tree-based methods apply a (random, possibly data dependent) linear projection at each node, with the differences between algorithms largely governed by the probability distribution from which projections are sampled. This general framework provides us a lens through which to study and improve existing ensemble tree-learning algorithms. A very sparse random projection preserves the desirable properties of axis-aligned decision trees, while mitigating their issues. Our statistically and computationally efficient parallelized R implementation is available on the Comprehensive R Archive Network (CRAN) (<https://cran.r-project.org/web/packages/rerf/>).

2 Background & Related Work

2.1 Statistical Learning: Classification and Regression

The classification problem is briefly described. Let $(X, Y) \sim f_{XY}$, where $X \in \mathcal{X} = \mathbb{R}^p$ is a random real-valued p -vector, $Y \in \mathcal{Y} = \{c_1, \dots, c_K\}$ is one of K categories or class labels associated with X , and f_{XY} is their joint distribution, which is generally unknown. In this work, we will use the lower case counterparts (x, y) to denote a particular realization of the random variable pair (X, Y) . Given a training set $D_n = \{X_i, Y_i\}_1^n \in \mathcal{D}_n$, the goal is to learn a classifier $h(\cdot|D_n) : \mathbb{R}^p \rightarrow \mathcal{Y}$ that correctly predicts the unobserved class label Y associated with an observed X . Specifically, we would like to minimize $P_{XY}(h(X|D_n) \neq Y)$, the probability of misclassification. It is well-known that the classifier $h^*(X) = \underset{k}{\operatorname{argmax}} P_{Y|X}(Y = k|X)$, known as the Bayes classifier, minimizes the probability of misclassification. For regression, instead let $Y \in \mathcal{Y} = \mathbb{R}$ be a real-valued response variable. The goal is then to learn a function $h(\cdot|D_n) : \mathbb{R}^p \rightarrow \mathcal{Y}$ that predicts a real-valued response Y associated with an observed X that minimizes the mean-squared generalization error $\mathbb{E}_{X,Y}[(Y - h(X|D_n))^2]$.

2.2 Random Forests

The original random forest (RF) procedure popularized by Leo Breiman is one of the most commonly employed classification learning algorithms. RF proceeds by building T decision trees via a series of recursive binary splits of the training data. The nodes in a tree are split into two daughter nodes by maximizing some notion of information gain, which typically reflects the reduction in class impurity of the resulting partitions. A common measure of information gain in decision trees is the decrease in Gini impurity, $I(S)$, for a set of observations S . The Gini impurity for classification is defined as $I(S) = \sum_{k=1}^K f_k(1 - f_k)$, where $f_k = \frac{1}{|S|} \sum_{i \in S} \mathbb{I}[y_i = k]$. Regression has an equivalent information gain counterpart; however, Breiman [2001] instead recommended the decrease in objective value as the splitting criteria, $I(S) = \sum_{y \in S} (y - \bar{y})^2$, where $\bar{y} = \frac{1}{|S|} \sum_{y \in S} y$, a recommendation that we follow here. Let $\theta = (j, \tau)$, where j is an index selecting a dimension and τ is a splitting threshold. Furthermore, let $\mathcal{S}^L(\theta) = \{i : x_i^{(j)} \leq$

$\tau, \forall i \in \mathcal{S}$ and $\mathcal{S}^R(\theta) = \{i : x_i^{(j)} > \tau, \forall i \in \mathcal{S}\}$ be the subsets of \mathcal{S} to the left and right of the splitting threshold, respectively. Here, $x_i^{(j)}$ denotes the value of the j th feature for the i th observation. A split is made on a "best" $\theta^* = (j^*, \tau^*)$ via the following optimization:

$$\theta^* = \underset{\theta}{\operatorname{argmax}} |\mathcal{S}|I(\mathcal{S}) - |\mathcal{S}^L(\theta)|I(\mathcal{S}^L(\theta)) - |\mathcal{S}^R(\theta)|I(\mathcal{S}^R(\theta)).$$

This optimization is carried out by exhaustively searching for the best split threshold τ^* over a random subset of the features. Specifically, a random subset of the p features is sampled. For each feature in this subset, the observations are sorted from least to greatest, and the split objective function is evaluated at each midway point between adjacent pairs of observations.

Nodes are recursively split until a stopping criteria is reached. Most commonly, the recursion stops when either a maximum tree depth is reached, a minimum number of observations in a node is reached, or a node is completely pure with respect to class label. The result of the tree induction algorithm is a set of split nodes and leaf nodes. The leaf nodes are disjoint partitions of the feature space \mathcal{X} , and each one is associated with a local prediction function. Let l_m be the m^{th} leaf node of an arbitrary classification or regression tree, and let $\mathcal{S}(l_m) = \{i : x_i \in l_m \forall i \in [n]\}$ be the subset of the training data contained in l_m . The local leaf prediction is:

$$h(l_m) = \underset{c_k \in \mathcal{Y}}{\operatorname{argmax}} \sum_{i \in \mathcal{S}(l_m)} \mathbb{I}[y_i = c_k] \quad (\text{classification}) \qquad h(l_m) = \frac{1}{|\mathcal{S}(l_m)|} \sum_{i \in \mathcal{S}(l_m)} y_i \quad (\text{regression})$$

A tree makes a prediction for a new observation x by moving the observation down the tree according to the split functions associated with each split node until a terminal leaf node is reached. Let $m(x)$ be the index of the leaf node that x falls into. Then the tree prediction is $h(l_{m(x)})$. Let $\hat{y}^{(t)}$ be the prediction made by the t^{th} tree. Then the prediction of the RF is the plurality vote (classification) or average (regression) of the predictions made by each tree:

$$\hat{y} = \underset{c_k \in \mathcal{Y}}{\operatorname{argmax}} \sum_{t=1}^T \mathbb{I}[\hat{y}^{(t)} = c_k] \quad (\text{classification}) \qquad \hat{y} = \frac{1}{|T|} \sum_{t=1}^T \hat{y}^{(t)} \quad (\text{regression})$$

For an ensemble classifier to perform well, the individual classifiers only need to classify better than chance, provided that their predictions have a sufficiently low level of correlation [Schapire, 1990]. RF decorrelates the trees via two mechanisms: (1) constructing each tree on a random bootstrap sample of the original training data and (2) restricting the optimization of the splitting dimension j over a random subset of the total p dimensions. The combination of these two randomizing effects typically leads to generalization performance much better than that of any individual tree [Breiman, 2001].

2.3 Recent Extensions to Random Forest

Various tactics have been employed to further promote the strength and diversity of trees. One feature of RF that limits both of these is its restriction of splits to be along the coordinate axes of the feature space. Therefore, one of the largest efforts for improving upon RFs has been in relaxing this restriction. The resulting forests are sometimes referred to as "oblique" decision forests, since the splits can be along directions oblique to the coordinate axes. Various approaches have been proposed for constructing oblique forests. Breiman [2001] proposed the

Forest-RC (F-RC) algorithm, which constructs d univariate projections, each projection a linear combination of L randomly chosen dimensions. The weights of each projection are independently sampled uniformly over the interval $[-1, 1]$. Strangely, Breiman’s F-RC never garnered the popularity that RF has acquired; the studies of both Breiman [2001] and Tomita *et al.* [2017] indicate that F-RC tends to empirically outperform RF on a wide variety of data sets. Heath *et al.* [1993] sample a randomly oriented hyperplane at each split node, then iteratively perturbs the orientation of the hyperplane until a good split is obtained. Rodriguez *et al.* [2006] attempt to find discriminative split directions via PCA. Menze *et al.* [2011] perform supervised learning of linear discriminative models at each node. Blaser and Fryzlewicz [2016] proposed the random rotation Random Forest (RR-RF) method, which uniformly randomly rotates the data prior to inducing each tree. Trees are then learned via the typical axis-aligned procedure on the rotated data. [Rainforth and Wood, 2015]’s Canonical Correlation Forests (CCFs) employ canonical correlation analysis at each split node in order to directly compute split directions that maximally correlate with the class labels. While the aforementioned approaches improve the flexibility of the learning procedure in seemingly different ways, they can be seen as different flavors of a more general learning procedure, which we elaborate on in Section 3.1.

2.4 Random Projections

Given a data matrix $\mathbf{X} \in \mathbb{R}^{n \times p}$, one can construct a random projection matrix $\mathbf{A} \in \mathbb{R}^{p \times d}$ whose entries a_{ij} are i.i.d. with zero mean and constant variance and multiply it by \mathbf{X} to obtain:

$$\tilde{\mathbf{X}} = \mathbf{X}\mathbf{A} \in \mathbb{R}^{n \times d}, \quad d \ll \min(n, p).$$

The much smaller matrix $\tilde{\mathbf{X}}$ preserves all pairwise distances of \mathbf{X} in expectation.

Due to theoretical guarantees, random projections are commonly employed as a dimensionality reduction tool in machine learning applications ([Bingham and Mannila, 2001; Fern and Brodley, 2003; Fradkin and Madigan, 2003; Achlioptas, 2003; Hegde *et al.*, 2008]). While zero mean and constant variance of the entries are the only necessary conditions for preserving pairwise distances, different probability distributions over the entries lead to different average errors and error tail bounds. Li *et al.* [2006] demonstrate that **very sparse random projections**, in which a large fraction of entries in \mathbf{A} are zero, can maintain high accuracy and significantly speed up the matrix multiplication by a factor of \sqrt{p} or more. Specifically, a very sparse random projection matrix is constructed by sampling entries a_{ij} with the following probability distribution:

$$a_{ij} = \begin{cases} +1 & \text{with prob. } \frac{1}{2s} \\ 0 & \text{with prob. } 1 - \frac{1}{s}, \\ -1 & \text{with prob. } \frac{1}{2s} \end{cases}, \quad \text{typically } s \gg 3$$

Dasgupta and Freund [2008] proposed Random Projection Trees, in which they sampled dense random projections in an unsupervised fashion to approximate low dimensional manifolds, and later for vector quantization [Dasgupta and Freund, 2009] and nearest neighbor search [Dasgupta and Sinha, 2013]. Our work is inspired by this work, but in a supervised setting.

2.5 Gradient Boosted Trees

Gradient boosted trees (GBTs) are another tree ensemble method commonly used for regression and classification tasks. Unlike in RFs, GBTs are learned in an iterative stage-wise manner by directly minimizing a cost function via gradient descent [Breiman and others, 1998; Friedman, 2001]. Despite the obvious differences in the learning procedures between GBTs and RFs, they tend to perform comparably. A study by Wyner *et al.* [2017] argues that RFs and GBTs are both successful for the same reason—namely that both are weighted ensembles of interpolating classifiers that learn local decision rules.

GBTs have recently seen a marked surge in popularity and have been components of many recent Kaggle competitions. This is in part due to their tendency to be accurate on a wide range of settings. Their popularity and success can also be attributed to the recent release of XGboost [Chen and Guestrin, 2016] and LightGBM [Ke *et al.*, 2017], which are two extremely fast and scalable open-source software implementations. Due to the success of GBTs in many data science applications, we compare the XGBoost implementation to our methods.

2.6 Forest Packing

Forest Packing is a post ‘forest growing’ process that reorganizes and compacts a forest to reduce prediction latency [Browne *et al.*, 2018b]. The common approach to reduce prediction time involves batching observations which allows for an orderly traversal of trees leading to improved memory access coherency and a higher operational intensity. This form of acceleration increases prediction throughput but also increases prediction latency, making this technique impractical for many popular real time workloads. Conversely, Forest Packing reduces prediction latency by making two improvements over unpacked forests: storing nodes in a memory retrieval-friendly structure and using a modern CPU friendly prediction algorithm.

Forest Packing improves the memory layout of forests by storing nodes likely to be used together near each other in memory and removing duplicated leaf nodes. Parent nodes are stored adjacent to their most likely to be used child node, which reduces retrieval time by improving memory coherence. The likeliness of a child node’s use is based on the size of splits during training; where the child node with higher cardinality is assumed to be the more likely to be traversed during inference. The second layout improvement halves tree memory requirements by removing redundant leaf nodes. This is possible because the number of unique leaf nodes equals the number of classes in the training data set and leaf nodes account for half of all nodes in a tree. This memory savings prevents the pollution of a CPU’s memory with duplicated information, thereby improving performance for subsequent predictions.

In addition to improving a forest’s memory layout, Forest Packing makes a slight, but critical, modification to the typical forest prediction algorithm in order to take advantage of modern CPU enhancements. Processing throughput is increased in modern CPUs through the use of multiple instruction pipelines and predictive memory retrieval—neither enhancement is useful for the normal prediction algorithm. To take advantage of these enhancements, Forest Packing traverses multiple trees in a round robin fashion to efficiently use the concurrent pipelines, thereby reducing both pipeline stalls and memory access latency. In addition, multiple trees are stored together in bins with the first couple of tree levels intertwined which improves multi-core execution and further improves use of the memory hierarchy.

3 Methods

3.1 Random Projection Forests

We propose a general decision forest framework called Random Projection Forest (RPF), which comprises any decision forest that recursively partitions the data via arbitrarily oriented hyper-planes. Let $\mathbf{X} \in \mathbb{R}^{p \times n}$ be the observed feature matrix of n samples, each p -dimensional. The key idea of RPF is that at each split node of the tree, we have a set of predictor data points, $\tilde{\mathbf{X}} = \{\mathbf{x}_s\}_{s \in \mathcal{S}_i^l} \in \mathbb{R}^{p \times S_i^l}$, in which $S_i^l = |\mathcal{S}_i^l|$ is the cardinality of the set of predictor data points at the i^{th} node of the l^{th} tree. Let $f_{\mathbf{A}}$ be the *projection distribution*. We sample a matrix $\mathbf{A} \sim f_{\mathbf{A}}$, where $\mathbf{A} \in \mathbb{R}^{p \times d}$, possibly in a data dependent fashion, which we use to randomly project the predictor matrix $\tilde{\mathbf{X}}$, yielding $\tilde{\tilde{\mathbf{X}}} = \mathbf{A}^T \tilde{\mathbf{X}} \in \mathbb{R}^{d \times S_i^l}$, where d is the dimensionality of the projected space. See Algorithms 1 and 2 for details. Table 1 summarizes previous projection distribution choices adopted by various decision forest algorithms.

The choice of projection distribution can significantly impact the strength and diversity of the trees and thus also affects the overall behavior of the ensemble. We note that Breiman’s original axis-aligned RF algorithm can be characterized as a particular case of RPFs: construct \mathbf{A} so that for each of the d columns, we sample a coordinate (without replacement), and put a 1 in that coordinate, and zeros elsewhere. Similarly, F-RC constructs \mathbf{A} by sampling a fixed number of coordinates (without replacement) for each of the d columns, and puts a value uniformly sampled from $[-1, 1]$ in each of those coordinates. Rotation forests construct \mathbf{A} from the top d principal components of the data $\tilde{\mathbf{X}}$ at a given node. RR-RF constructs \mathbf{A} by uniformly randomly rotating the original input space for each tree. CCF for a univariate output constructs \mathbf{A} from the projections found by canonical correlation analysis (CCA). Thus, the key difference in all of these approaches is the choice of projection distribution.

While the best specification of a projection distribution (if one exists) is data set dependent, it is unreasonable and/or undesirable to try more than a handful of different cases. Therefore, for general purpose classification we advocate for a default projection distribution based on the following desiderata:

- **Strong and Diverse Trees.** While RF empirically performs well in many settings, it is quite restrictive in the sense that candidate splits evaluated at each node are constrained to be axis-aligned. Relaxing this geometric constraint may lead to trees that are both stronger and less correlated with one another.
- **Flexible Sparsity.** Tomita *et al.* [2017] demonstrated that F-RC empirically performed much better than RR-RF. The main difference between F-RC and RR-RF is that F-RC samples directions defined by linear combinations of only L inputs (a parameter to be specified by the user), whereas in RR-RF split directions are fully *dense* linear combinations. Thus, it seems that proper control of the sparsity of the random matrix \mathbf{A} is necessary when noisy and/or irrelevant dimensions are prevalent.
- **Interpretability.** Certain applications require interpretability, in addition to accuracy. While RF models can be complicated, suitable measures have been proposed to assess the relative contribution (importance) of each feature. This becomes prohibitive to compute for oblique forests if the space of possible split projections is not sufficiently constrained.

- **Expediency and Scalability.** Existing oblique forest algorithms typically involve expensive computations to identify and select splits, rendering them less space and time efficient than RF, and/or lack parallelized implementations.

3.2 Lumberjack

With these in mind, we developed a special case of RPF using very sparse random projections [Li *et al.*, 2006] as the projection distribution. Specifically, rather than sampling d non-zero elements of \mathbf{A} and enforcing that each column gets a single non-zero number (without replacement) as RF does, we relax these constraints and sample $\lceil \lambda p d \rceil$ non-zero numbers from $\{-1, +1\}$ with equal probabilities, where $\lambda \in (0, 1]$ is the density (fraction of nonzeros) of \mathbf{A} and $\lceil \cdot \rceil$ is the ceiling function.¹ These nonzeros are then distributed uniformly at random in \mathbf{A} . We refer to this particular variant of RPFs as “Lumberjack” because we demonstrate empirically that it tends to outperform other tree ensemble methods across a wide variety of data sets.

Figure 1 offers geometric intuition of how Lumberjack addresses the first two issues above (strong/diverse trees and flexible sparsity; interpretability and computational properties are addressed in Sections 5.5 and 7). Two simulated classification problems are constructed in which two classes lie in parallel hyperplanes in 20 dimensions. In one problem, which we will call the sparse problem, only the first two dimensions are informative of the class label. Furthermore, neither one of the first two dimensions are individually strongly informative. Specifically, class 0 is uniformly distributed on the noisy hyperplane $X_1 + X_2 = -\epsilon$, where $\epsilon \sim N(0.1, 0.01)$ is a small amount of independent Gaussian noise. Each of $X_1, X_3, \dots, X_{20} \stackrel{iid}{\sim} U(-0.5, 0.5)$, and X_2 is distributed according to the (noisy) hyperplane constraint. The distribution of class 1 is the same as that for class 0, except that the hyperplane is defined as $X_1 + X_2 = +\epsilon$. In the second problem, which we will call the dense problem, all dimensions are jointly informative of the class label, while no dimension is individually strongly informative. Specifically, class 0 is uniformly distributed on the noisy hyperplane $X_1 + \dots + X_{20} = -\epsilon$, where ϵ is distributed as in the sparse problem. Each of $X_1, \dots, X_{19} \stackrel{iid}{\sim} U(-0.5, 0.5)$, and X_{20} is distributed according to the (noisy) hyperplane constraint. The distribution of class 1 is the same as that for class 0, except that the hyperplane is defined as $X_1 + \dots + X_{20} = +\epsilon$.

The best projections found by RF, Lumberjack, and RR-RF at the root node were compared. For Lumberjack we set λ to $1/20$. We searched over all 20 dimensions for RF, while 8000 univariate random projections were evaluated for Lumberjack and RR-RF.² RF cannot find a good projection in the sparse problem because no dimension is marginally informative. RR-RF samples projections uniformly over the 20-dimensional hypersphere, and thus any projection it samples is very likely to be nearly orthogonal to the optimal projection [Vershynin, 2017]. Lumberjack is the only one that can find a good projection in the sparse case. For the dense problem, Lumberjack struggles because of the sparsity constraint on the distribution of \mathbf{A} . However, RR-RF, which does not constrain sparsity, still struggles for the same reason as in the sparse problem. To summarize, in moderate or high dimensional problems, biasing projections to be sparse can significantly improve the probability of finding a discriminative projection if the true underlying decision boundary is sparse. At the same time, if the true underlying decision boundary is dense, then neither sparse nor dense random projections are likely to have

¹While λ can take a value of one, we only try values up to $5/p$ in our experiments.

²RR-RF typically performs a single rotation of the data for each tree. Here we sampled a random rotation matrix 400 times, such that 8000 univariate projections were evaluated.

Algorithm	$f_{\mathbf{A}}$	Ref
RF	Let $\{j_k\}_{k=1}^d$ be a set of indices obtained by sampling without replacement from $\{1, \dots, p\}$. Let \mathbf{e}_i be the i th column of the $p \times p$ identity matrix. Then $\mathbf{A} = [\mathbf{e}_{j_1} \mathbf{e}_{j_2} \dots \mathbf{e}_{j_d}]$.	Breiman [2001]
F-RC	Let a_{ij} denote the element corresponding to the i th row and j th column of \mathbf{A} . For each $j \in \{1, \dots, d\}$, let S_j^L be a set of L indices obtained by sampling without replacement from $\{1, \dots, p\}$. Then $a_{ij} \stackrel{iid}{\sim} U(-1, 1) \forall i \in S_j^L$, and $a_{ij} = 0 \forall i \notin S_j^L$.	Breiman [2001]
RR-RF	Let \mathbf{R} be a $p \times p$ uniformly random rotation matrix. Then $\mathbf{A} = \mathbf{R}\mathbf{A}_{RF}$, where \mathbf{A}_{RF} is a random matrix sampled from the $f_{\mathbf{A}}$ defined for RF above.	Blaser and Fryzlewicz [2016]
Rot-For	Let $\mathbf{X} \in \mathbb{R}^{n \times p}$ be the input data matrix at a split node. Let $S_j \forall j \in \{1, \dots, K\}$ be uniformly random disjoint subsets of the column indices $\{1, \dots, p\}$, and let each $\mathbf{I}'_j \forall j \in \{1, \dots, K\}$ be a copy of the identity matrix such that the columns indexed by S_j are zeroed out. Then $\mathbf{A} = [PCA(\mathbf{X}\mathbf{I}'_1) \ PCA(\mathbf{X}\mathbf{I}'_2) \ \dots \ PCA(\mathbf{X}\mathbf{I}'_K)]$, where $PCA(\cdot)$ returns the matrix of principal components having nonzero eigenvalues.	Rodriguez <i>et al.</i> [2006]
O-RF	Let $\mathbf{X} \in \mathbb{R}^{n \times p}$ be the input data matrix at a split node and $\mathbf{y} \in \{0, 1\}^{n \times 1}$ be corresponding class labels. Let \mathbf{I}' be a copy of the $p \times p$ identity matrix with L columns – chosen at random – zeroed out. Then $\mathbf{A} = RIDGE(\mathbf{X}\mathbf{I}', \mathbf{y})$, where $RIDGE(\cdot)$ returns the vector projection found by ridge logistic regression.	Menze <i>et al.</i> [2011]
CCF	Let $\mathbf{X} \in \mathbb{R}^{n \times p}$ be the input data matrix at a split node and $\mathbf{y} \in \{0, 1\}^{n \times 1}$ be corresponding class labels. Define $\tilde{\mathbf{X}} \in \mathbb{R}^{m \times p}, m < n$ to be a data matrix corresponding to a random subset of m of the node observations. Let \mathbf{I}' be a copy of the $p \times p$ identity matrix with L columns – chosen at random – zeroed out. Then $\mathbf{A} = CCA(\tilde{\mathbf{X}}\mathbf{I}', \mathbf{y})$, where $CCA(\cdot)$ returns the matrix of column-wise projections found by canonical correlation analysis.	Rainforth and Wood [2015]

Table 1: A summary of the random projection matrix distribution $f_{\mathbf{A}}$ adopted by previously proposed decision forest algorithms. Note that this list is not exhaustive. We use the notation $[\mathbf{A}_1 \ \mathbf{A}_2 \ \mathbf{A}_3]$ to denote a matrix defined by the column-wise concatenation of the matrices (or column vectors) $\mathbf{A}_1, \mathbf{A}_2$, and \mathbf{A}_3

good discrimination. This is due to the fact that in even moderate dimensions, there is a lot more room, which translates to a lot more opportunities for vectors to be orthogonal. One can simply sample more projections to increase the probability of finding a discriminative one, but this becomes prohibitive computationally. This further supports the adoption of Lumberjack with high sparsity as a default projection distribution for RPF.

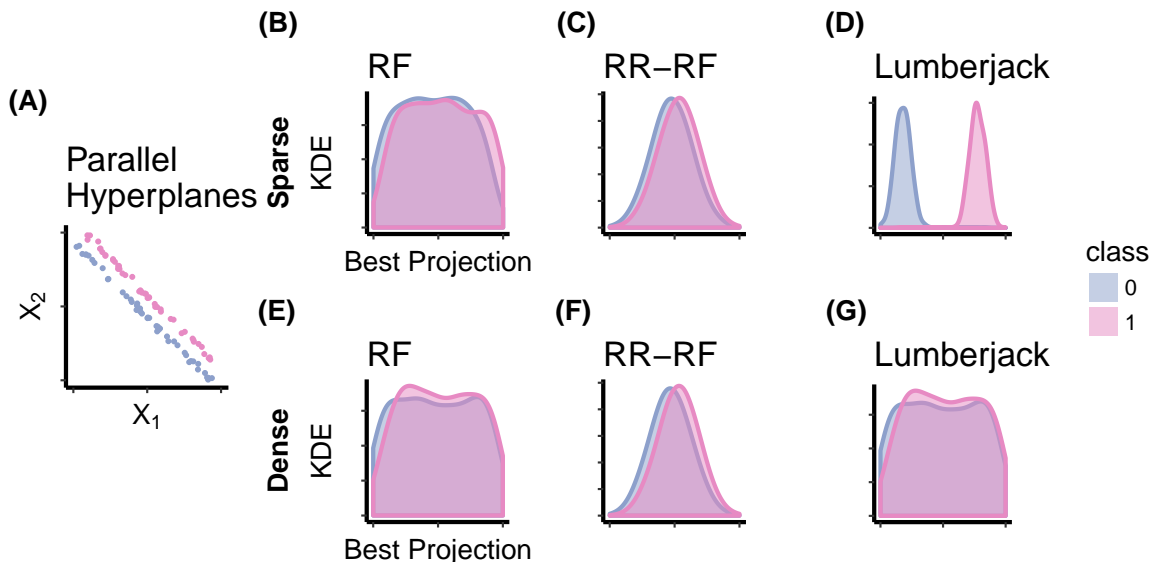


Figure 1: Comparison of the best projections found by Lumberjack, RR-RF, and RF on the sparse **(B-D)** and dense **(E-G)** 20-dimensional parallel hyperplanes synthetic data sets. The key difference between the sparse and dense problems is that class membership is determined by only the first two dimensions in the former and by all dimensions in the latter (see Section 3.1 for distributional details). **(A)** A random sample of the parallel hyperplanes data in two dimensions. **(B-D)** Best projection sampled by RF, RR-RF, and Lumberjack at the root node, respectively on the sparse problem. 8000 projections were sampled. For each class, we show a kernel density estimate of posterior distribution after projection averaged over 50 repeated experiments. Lumberjack is the only one that is able to find a discriminating projection with high probability when no dimension is individually informative and there are many uninformative dimensions. **(E-G)** The same as the previous three panels, except for the dense problem. When no dimension is individually informative and all dimensions are jointly informative, no method can find a discriminating projection with high probability using the specified hyper-parameter values.

3.3 Implementation Details

We use our own R implementation for evaluations of RF, Lumberjack, F-RC, and RR-RF [Browne *et al.*, 2018a]. It was more difficult to modify one of the existing popular tree learning implementations due to the particular way in which they operate on the input data. In all of the popular axis-aligned tree learning implementations, each feature in the input data matrix is sorted just once prior to inducing a tree, and the tree induction procedure operates directly on this pre-sorted data. Since trees in a RPF, in general, are constructed by splitting on new features consisting of linear combinations of the original dimensions, which are not known a priori, we cannot operate on a single presorted data matrix. Therefore our implementation is written from scratch in mostly native R. The code has been extensively profiled and optimized for speed and memory performance. Profiling revealed the primary performance bottleneck to be the portion of code responsible for finding the best split. In order to improve speed, this portion of code was implemented in C++ and integrated into R using the Rcpp package [Eddelbuettel, 2018]. Further speedup is achieved through multicore parallelization of tree construction and

byte-compilation via the R compiler package.

XGBoost is evaluated using the R implementation available on CRAN [Chen, 2018]. CCF is evaluated using the authors' openly available MATLAB implementation [Rainforth and Wood, 2015].

3.4 Training and Hyperparameter Tuning

Unless otherwise stated, model training and tuning for all algorithms except for XGBoost and CCF is performed in the following way. The number of trees used for each algorithm is 500. This number of trees was empirically determined to be sufficient for convergence of out-of-bag error in classification for all methods (not shown). In regression, the number of trees above 100 didn't vary empirical results thus we adopted 500 trees in regression as well. In all methods, trees are fully grown unpruned (that is, nodes are split until pure). The split objective is to maximize the reduction in Gini impurity in classification and split-wise MSE in regression. Two hyperparameters are tuned via minimization of out-of-bag error in classification. We plan to tune hyperparameters for regression in future work. The first parameter tuned is d , the number of candidate split directions evaluated at each split node. Each algorithm is trained for $d = p^{1/4}$, $p^{1/2}$, $p^{3/4}$, and p . Additionally, Lumberjack and F-RC are trained for $d = p^2$. For RF, d is restricted to be no greater than p by definition. The second hyperparameter tuned is λ , the average sparsity of univariate projections sampled at each split node. The values optimized over for Lumberjack and F-RC are $\{1/p, \dots, 5/p\}$. Note, for RF λ is fixed to $1/p$ by definition, since the univariate projections are constrained to be along one of the coordinate axes of the data.

For CCF, the number of trees is 500, trees are fully grown, and the split objective is to maximize the reduction in class entropy (this is the default objective found to perform best by the authors). Projection bootstrapping is used rather than bagging [Rainforth and Wood, 2015]. The only hyperparameter tuned is the number of features subsampled prior to performing CCA. We optimize this hyperparameter over the set $\{p^{1/4}, p^{1/2}, p^{3/4}, p\}$. The projection bootstrapping procedure requires each tree to be trained on the full data set. Since there are no out-of-bag samples for each tree, selection of the best value is based on minimization of a five-fold cross-validation error rate instead.

Hyperparameters in XGBoost are tuned via grid search using the R caret package (see Appendix A for details).

4 Real Data Empirical Performance

4.1 Lumberjack Exhibits Best Overall Classification Performance on a Large Suite of Benchmark data sets

Lumberjack compares favorably to RF, XGBoost, RR-RF, and CCF on a suite of 105 benchmark data sets from the UCI machine learning repository (Figure 2). This benchmark suite is a subset of the same problem sets previously used to conclude RF outperformed >100 other algorithms [Fernandez-Delgado *et al.*, 2014] (16 were excluded for various reasons; see Section B for preprocessing details).

Figure 2 shows pairwise comparisons of Lumberjack with RF (dark gray), XGBoost (pink), RR-RF (blue), and CCF (purple) on the UCI data sets. For each data set, the square root of the difference in error rates (normalized by the chance error rate) between the algorithms is

plotted against the square root of the average of their error rates. Error rates are estimated for each algorithm for each data set via five-fold cross-validation. The difference in error rates on a particular data set were computed for each fold and the average then taken over the folds. Comparisons are shown for the 65 numeric data sets, the 40 data sets having at least one categorical feature, and all 105 data sets in Figures 2(A-C), respectively. A positive value on the y-axis indicates that Lumberjack performed better than the algorithm it is being compared to on a particular data set, while a negative value indicates it performed worse. As indicated by the upward skews of the histograms of differences in errors shown on the right margins, Lumberjack tends to outperform all four other algorithms over all data sets, in particular, due to its relative performance on the numeric data sets. This is despite the fact that XGBoost is tuned significantly more than Lumberjack in these comparisons (see 3.4 for details). Wilcoxon signed-rank tests produce p-values < 0.005 for all data sets and just the numeric ones against each of the reference methods. Lumberjack performs disproportionately better on the numeric data sets than on the categorical data sets for all pair-wise algorithm comparisons, except for the comparison with CCF. The data sets having categorical features had to undergo more processing due to one-hot encoding of the categorical features. Also, the categorical data sets prior to preprocessing tended to have relatively more missing data than the other data sets. It is possible that this heavier processing of the categorical data sets introduces additional noise.

While the hyperparameters λ and d of Lumberjack were tuned in this comparison, default hyperparameters can be of great value to researchers who use Lumberjack out of the box. This is especially true for those not familiar with the details of a particular algorithm or those having limited time and computational budget. Therefore, we sought suitable default values for λ and d based on classification performance on the UCI data sets. For each data set, for each fold the hyperparameter settings are ranked based on error rate on the held out set. A rank of n indicates n^{th} place (i.e. first place indicates lowest error rate). Ties in the ranking procedure are handled by assigning all ties the same averaged rank. For example, consider the set of real numbers $\{a_1, a_2, a_3\}$ such that $a_1 > a_2 = a_3$. Then a_1 would be assigned a rank of three and a_2 and a_3 would both be assigned a rank of $(1 + 2)/2 = 1.5$. The rank of each hyperparameter pair was averaged over the five folds. Finally, for each hyperparameter pair, the median rank is computed over the data sets. The median rank for each hyperparameter setting is depicted in Figure 3. The results here suggest that $d = p^2$ and $\lambda = 4/p$ is the best default setting for Lumberjack with respect to classification performance. However, we choose the setting $d = p$ and $\lambda = 3/p$ as the default values in our implementation because it requires substantially less training time for moderate to large p at the expense of only a slightly greater tendency to perform worse on the UCI data sets.

Table 3 (Appendix D) compares Lumberjack to RF and CCF on 42 WEKA regression data sets from the study by Rainforth and Wood [2015]. The performance of all three algorithms is approximately the same on data sets where only numerical variables are present. Performance of Lumberjack is notably worse than the other baseline methods (CCF, RF) when a mixture of categorical and numerical variables are in the data set. The tendency of Lumberjack to perform worse when categorical variables are in the data set was also observed in the empirical classification benchmarks.

5 Numerical Analysis of Lumberjack

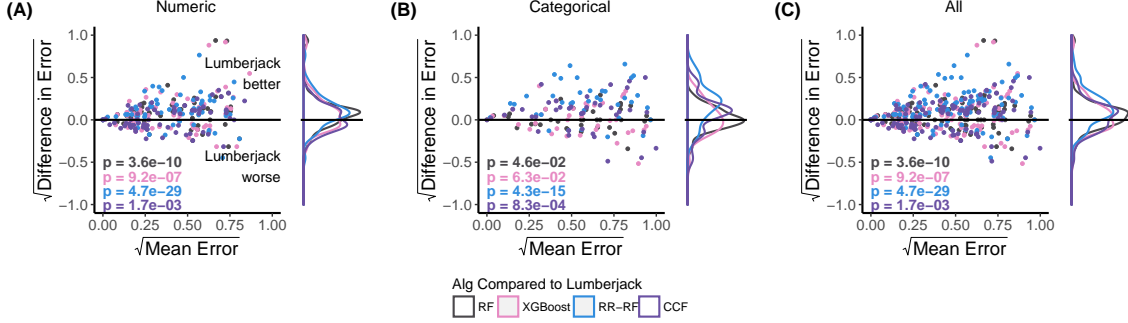


Figure 2: Pairwise comparisons of Lumberjack with RF, XGBoost, RR-RF, and CCF on the (A) numeric, (B) categorical, and (C) all (numeric and categorical combined) 105 data sets from the UCI Machine Learning Repository. For each data set, the square root of the difference in error rates (normalized by chance error) between the algorithms (y-axis) are plotted against the square root of the average of their normalized error rates (x-axis). A positive value on the y-axis indicates Lumberjack has a lower error rate than the algorithm it is being compared to. Kernel density estimates (KDEs) of the distributions of the differences in errors are shown on the right margins. The skew of the KDEs to the top in addition to left-tailed Wilcoxon signed-rank tests indicate that overall, Lumberjack tends to perform better than the other algorithms.

5.1 Simulated data sets

In the sections that follow, we perform a variety of experiments on three carefully constructed simulated classification problems, which we refer to as **Sparse Parity**, **Orthant**, and **Trunk**. These constructions are chosen to highlight various properties of different algorithms and gain insight into their behavior.

Sparse Parity is a multivariate generalization of the noisy XOR problem. It is a p -dimensional two-class problem in which the class label is 0 if the number of dimensions having positive values amongst the first $p^* < p$ dimensions is even and 1 otherwise. Thus, only the first p^* dimensions carry information about the class label, and no individual dimension contains any information. Specifically, let $X = (X_1, \dots, X_p)$ be a p -dimensional feature vector, where each $X_1, \dots, X_p \stackrel{iid}{\sim} U(-1, 1)$. Furthermore, let $S = \sum_{j=1}^{p^*} \mathbb{I}(X_j > 0)$, where $p^* < p$ and $\mathbb{I}(X_j > 0)$ is the indicator that the j th feature of a sample point x has a value greater than zero. A sample's class label Y is equal to the parity of S . That is, $Y = \text{odd}(S)$, where odd returns 1 if its argument is odd and 0 otherwise. The Bayes optimal decision boundary for this problem is a union of hyperplanes aligned along the first p^* dimensions. For the experiments presented in the following sections, $p^* = 3$ and $p = 20$. Figure 4 (A,B) show cross-sections of the first two dimensions taken at two different locations along the third dimension.

Orthant is a multi-class problem in which the class label is determined by the orthant in which a datapoint resides. A key characteristic of this problem is that the individual dimensions are strongly and equally informative. An orthant in \mathbb{R}^p is a generalization of a quadrant in \mathbb{R}^2 . In other words, it is a subset of \mathbb{R}^p defined by constraining each of the p coordinates to be positive or negative. For instance, in \mathbb{R}^2 , there are four such subsets: $X = (X_1, X_2)$ can either be in 1) $\mathbb{R}^+ \times \mathbb{R}^+$, 2) $\mathbb{R}^- \times \mathbb{R}^+$, 3) $\mathbb{R}^- \times \mathbb{R}^-$, or 4) $\mathbb{R}^+ \times \mathbb{R}^-$. Note that the number of orthants in p dimensions is 2^p . Specifically for our experiments, we sample each $X_1, \dots, X_p \stackrel{iid}{\sim} U(-1, 1)$. Associate a unique integer index from 1 to 2^p with each orthant, and let $O(X)$ be the index of

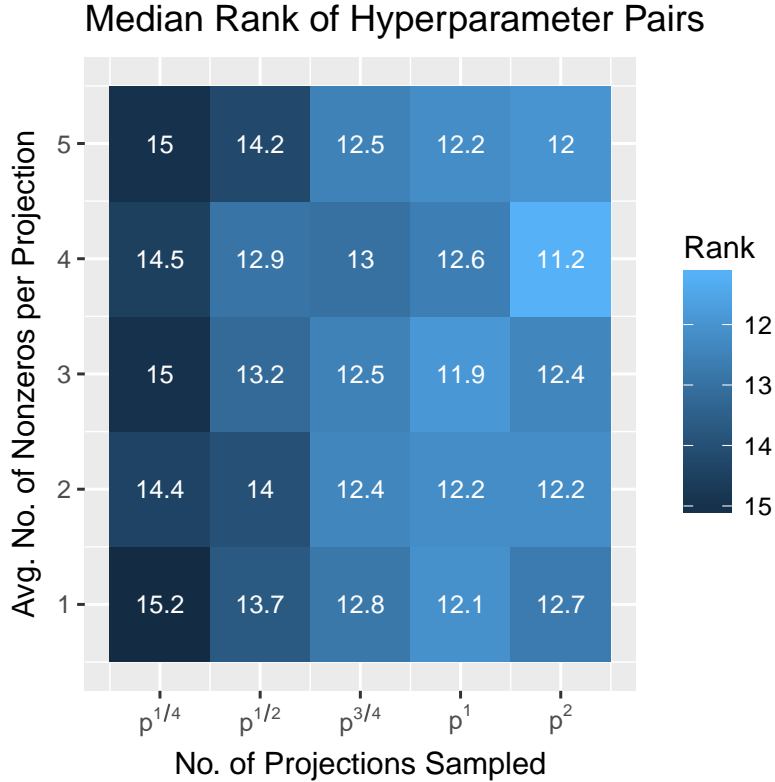


Figure 3: Median rank of Lumberjack’s (d, λ) hyperparameter pairs on the UCI classification data sets (lower is better). Although $(p^2, 4/p)$ is the best performance-wise, we select $(p, 3/p)$ as the default because of a good balance between accuracy and training time.

the orthant in which X resides. The class label is $Y = O(X)$. Thus, there are 2^p classes. The Bayes optimal decision boundary in this setting is a union of hyperplanes aligned along each of the p dimensions. We set $p = 6$ in the following experiments. Figure 4 (D,E) show cross-sections of the first two dimensions taken at two different locations along the third dimension.

Trunk is a balanced two-class problem in which each class is distributed as a p -dimensional multivariate Gaussian with identity covariance matrices [Trunk, 1979]. Every dimension is informative, but each subsequent dimension is less informative than the last. The means of class 1 and 0 are $\mu_1 = (1, \frac{1}{\sqrt{2}}, \frac{1}{\sqrt{3}}, \dots, \frac{1}{\sqrt{p}})$ and $\mu_0 = -\mu_1$, respectively. The Bayes optimal decision boundary is the hyperplane $(\mu_1 - \mu_0) \cdot X = 0$. We set $p = 10$ in the following experiments.

5.2 Simulated Performance

We compare error rates of RF, Lumberjack, F-RC, and CCF on the sparse parity and orthant problems. Error rates are estimated by taking a random sample of size n , training the classifiers, and computing the fraction misclassified in a test set of 10,000 samples. This is repeated ten times for each value of n . The reported error rate is the mean over the ten repeated experiments.

Lumberjack performs as well as or better than the other algorithms on both the sparse parity (Figure 4A-C) and orthant problems (Figure 4D-F). RF performs relatively poorly on the sparse

parity problem. Although the optimal decision boundary is a union of axis-aligned hyperplanes, each dimension is completely uninformative on its own. Since axis-aligned partitions are chosen one at a time in a greedy fashion, the trees in RF struggle to learn the correct partitioning. On the other hand, oblique splits are informative, which substantially helps the generalization ability of Lumberjack and F-RC. While F-RC performs well on the sparse parity problem, it performs much worse than RF and Lumberjack on the orthant problem. On the orthant problem, in which RF is designed to do exceptionally well, Lumberjack performs just as well. CCF performs poorly on both problems, which may be due to the fact that CCA is not optimal for the particular data distributions. For instance, in the sparse parity problem, the projection found by CCA at the first node is approximately the difference in class-conditional means, which is zero. Furthermore, CCF only evaluates $d = \min(l, C - 1)$ projections at each split node, where l is the number of dimensions subsampled and C is the number of classes. On the other hand, Lumberjack evaluates d random projections, and there is no limit on d . Overall, Lumberjack is the only method of the four that performs on all of the simulated data settings.

A key difference between the default distribution of Lumberjack and F-RC is that F-RC requires specification of a hyperparameter that fixes the sparsity of the sampled univariate (vector) projections. Lumberjack on the other hand, requires specification of a sparsity on the entire random matrix \mathbf{A} , and hence, only an *average* sparsity on the univariate projections. In other words, Lumberjack induces a probability distribution on the sparsity of univariate projections, whereas F-RC does not. An implication of this is that if the Bayes optimal decision boundary is locally sparse, misspecification of the hyperparameter controlling the sparsity of \mathbf{A} may be more detrimental to F-RC than Lumberjack. Therefore, we examine the sensitivity of classification performance of Lumberjack and F-RC to λ on the simulated data sets previously described. For each of $\lambda \in \{\frac{1}{p}, \dots, \frac{5}{p}\}$, the best performance for each algorithm is selected with respect to the hyperparameter d based on minimum out-of-bag error. Error rate on the test set is computed for each of the five hyperparameters for the two algorithms. Figure 5 shows the dependence of error rates of Lumberjack and F-RC on λ for the sparse parity ($n = 5,000$) and orthant ($n = 400$) settings. The $n = 5,000$ setting for Sparse Parity was chosen because both F-RC and Lumberjack perform well above chance (see Figure 4C). The $n = 400$ setting for Orthant was chosen for the same reason and also because it displays the largest difference in classification performance in Figure 4F. In both settings, Lumberjack is more robust to the choice in λ than is F-RC.

5.3 Strength and Correlation of Trees

One of the most important and well-known results in ensemble learning theory for classification states that the generalization error of an ensemble learning procedure is bounded above by the quantity $\bar{\rho}(1 - s^2)/s^2$, where $\bar{\rho}$ is a particular measure of the correlation of the base learners and s is a particular measure of the strength of the base learners [Breiman, 2001]. In both Lumberjack and F-RC, the set of possible splits that can be sampled is far larger in size than that for RF, which may lead to more diverse trees. Moreover, the ability to sample a more diverse set of splits may increase the likelihood of finding good splits and therefore boost the strength of the trees. To investigate the strength and correlation of trees using different projection distributions, we evaluate RF, F-RC, and Lumberjack on the three simulation settings described above. Scatter plots of tree strength vs tree correlation are shown in Figure 6 for sparse parity ($n = 1000$), orthant ($n = 400$), Trunk ($n = 10$), and Trunk ($n = 100$). In all four settings, Lumberjack classifies as well as or better than RF and F-RC.

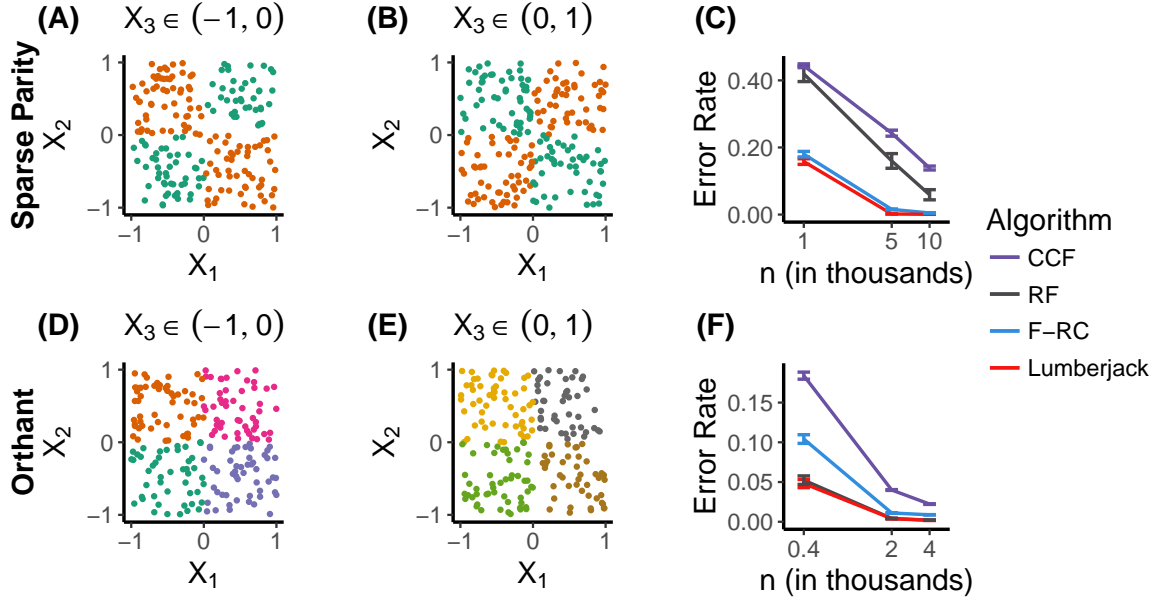


Figure 4: Classification performance on the sparse parity ($p = 20$) and orthant ($p = 6$) problems for various numbers of training samples. F-RC has been known to perform much better than RF on the sparse parity problem [Tomita *et al.*, 2017]. The orthant problem is designed for RF to perform well because the optimal splits are axis-aligned. **(A)** A cross-section of the first two dimensions of sparse parity when $X_3 \in (-1, 0)$. Each of $X_1, \dots, X_{20} \stackrel{iid}{\sim} U(-1, 1)$. Only the first three dimensions are informative w.r.t. class label. **(B)** The same as (A), except that the cross-section is taken over $X_3 \in (0, 1)$. **(C)** Error rate plotted against the number of training samples for sparse parity. Error rate is the average over ten repeated experiments. Error bars indicate the standard error of the mean. **(D)** A cross-section of the first two dimensions of orthant when $X_3 \in (-1, 0)$. Each of $X_1, \dots, X_6 \stackrel{iid}{\sim} U(-1, 1)$. All dimensions are required to determine the class label, since each orthant corresponds to a different class. **(E)** The same as (D), except that the cross-section is taken over $X_3 \in (0, 1)$. **(F)** The same as (C), except for orthant. Lumberjack is the only method of the four that performs well across all simulated data settings.

Figure 6(A) shows that on the sparse parity data set, Lumberjack and F-RC produce significantly stronger trees than does RF, at the expense of an increase in correlation amongst the trees. Noting that both Lumberjack and F-RC are much more accurate than RF in this setting, any performance degradation due to the increase in correlation relative to RF is outweighed by the increased strength. Lumberjack produces slightly less correlated trees than does F-RC, which may explain why Lumberjack has a slightly lower error rate than does F-RC on this setting.

Figure 6(B) shows that on the orthant data set, F-RC produces trees of roughly the same strength as those in RF, but significantly more correlated. This may explain why F-RC has substantially worse prediction accuracy than does RF. Lumberjack also produces trees more correlated than those in RF, but to a lesser extent than F-RC. Furthermore, the trees in Lumberjack are stronger than those in RF. Observing that Lumberjack has roughly the same error rate as RF does, it seems that any contribution of greater tree strength in Lumberjack is canceled

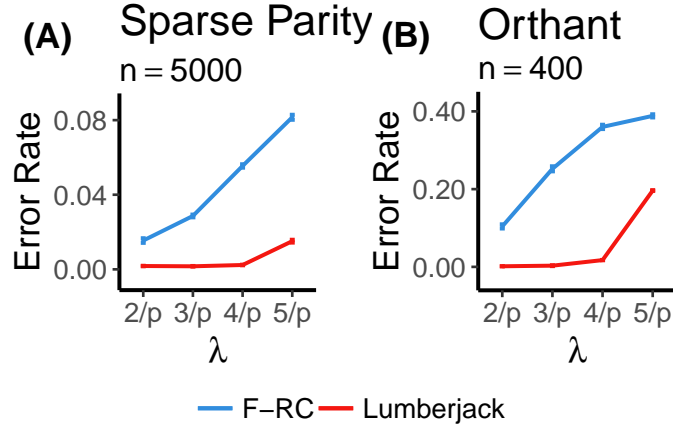


Figure 5: Dependence of error rate on the hyperparameter λ , which controls the average density (sparsity) of projections for two different simulation settings. **(A)** Error rate as a function of λ on sparse parity ($p = 20$). **(B)** The same as (A) except on orthant ($p = 6$). In both cases, Lumberjack is less sensitive to different values of λ than is F-RC.

by a contribution of greater tree correlation.

In Figure 6(C), we see that on the Trunk problem with $p = 10$ and $n = 10$, Lumberjack and F-RC produces trees that are comparable in strength to those in RF but less correlated. However, when increasing n to 100, shown in Figure 6(D), the trees in Lumberjack and F-RC become both stronger and more correlated. In both cases, Lumberjack and F-RC have better classification performance than RF.

The results shown in Figure 6(C,D) suggest a possibly general phenomenon. Namely, for smaller training set sizes, tree correlation may be a more critical factor than tree strength because their simply is not enough data to induce strong trees, and thus, the only way to improve performance is through increasing the diversity of trees. Likewise, when the training set is sufficiently large, tree correlation matters less because there is enough data to induce strong trees. Since Lumberjack has the ability to produce both stronger and more diverse trees than RF, it is adaptive to both regimes. In all four settings, Lumberjack never produces more correlated trees than does F-RC, and sometimes produces less correlated trees. A possible explanation for this is that the splits made by Lumberjack are linear combinations of a random number of dimensions, whereas in F-RC the splits are linear combinations of a fixed number of dimensions. Thus, in some sense, there is more randomness in Lumberjack than in F-RC.

5.4 Understanding the Bias and Variance of Lumberjack

The crux of supervised learning tasks is to optimize the trade-off between bias and variance. As a first step in understanding how the choice of projection distribution effects the balance between bias and variance, we estimate bias, variance, and error rate of the various algorithms on the sparse parity problem. Universally agreed upon definitions of bias and variance for 0-1 loss do not exist, and several such definitions have been proposed for each. Here we adopt the framework for defining bias and variance for 0-1 loss proposed in James [2003]. Under this framework, bias and variance for 0-1 loss have similar interpretations to those for mean squared error. That is, bias is a measure of the distance between the expected output of a

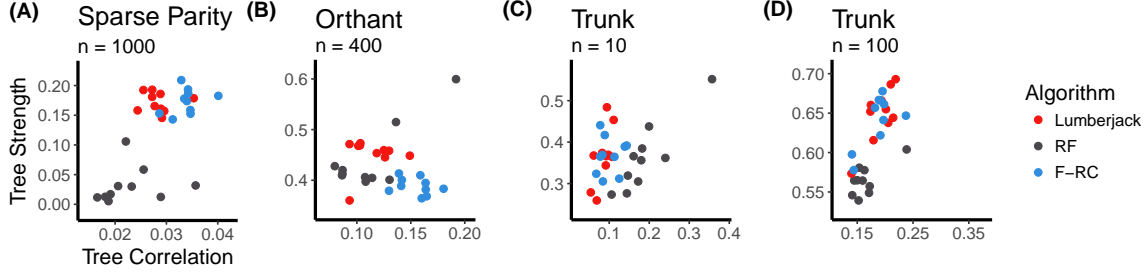


Figure 6: Comparison of tree strength and correlation of Lumberjack, RF, and F-RC on four of the simulated data sets: **(A)** sparse parity with $p = 10, n = 1000$, **(B)** orthant with $p = 6, n = 400$, **(C)** Trunk with $p = 10, n = 10$, and **(D)** Trunk with $p = 10, n = 100$. For a particular algorithm, there are ten dots, each corresponding to one of ten trials. Note in all settings, Lumberjack beats RF and/or F-RC. However, the mechanism by which it does varies across the different settings. In sparse parity Lumberjack wins because the trees are substantially stronger, even though the correlation increases. In Trunk for small sample size, it is purely because of less correlated trees. However, when sample size increases 10-fold, it wins purely because of stronger trees. This suggests that Lumberjack can effectively trade-off strength for correlation on the basis of sample complexity to empirically outperform RF and F-RC.

classifier and the true output, and variance is a measure of the average deviation of a classifier output around its expected output. Unfortunately, these definitions (along with the term for Bayes error) do not provide an additive decomposition for the expected 0-1 loss. Therefore, James [2003] provides two additional statistics that do provide an additive decomposition. In this decomposition, the so-called "systematic effect" measures the contribution of bias to the error rate, while the "variance effect" measures the contribution of variance to the error rate. For completeness, we restate these definitions below.

Let $\bar{h}(X) = \underset{k}{\operatorname{argmax}} P_{D_n}(h(X|D_n) = k)$ be the most common prediction (mode) with respect to the distribution of D_n . This is referred to as the "systematic" prediction in James [2003]. Furthermore, let $P^*(X) = P_{Y|X}(Y = h^*(X)|X)$ and $\bar{P}(X) = P_{D_n}(h(X|D_n) = \bar{h}(X))$. The bias, variance, systematic effect (SE), and variance effect (VE) are defined as

$$\begin{aligned}
 \text{Bias} &= P_X(\bar{h}(X) = h^*(X)), \\
 \text{Var} &= 1 - E_X[\bar{P}(X)], \\
 \text{SE} &= E_X[P^*(X) - P_{Y|X}(Y = \bar{h}(X)|X)], \\
 \text{VE} &= E_X[P_{Y|X}(Y = \bar{h}(X)|X) \\
 &\quad - \sum_k P_{Y|X}(Y = k|X)P_{D_n}(h(X|D_n) = k)].
 \end{aligned}$$

Figure 7 compares estimates of bias, variance, variance effect, and error rate for Lumberjack, RF, and F-RC as a function of number of training samples. Since the Bayes error is zero in these settings, systematic effect is the same as bias. The four metrics are estimated from 100 repeated experiments for each value of n . In Figure 7(A), Lumberjack has lower bias than both RF and F-RC for all training set sizes. All algorithms converge to approximately zero bias after about 3000 samples. Figure 7(B) shows that RF has substantially more variance than do Lumberjack and F-RC, and Lumberjack has slightly less variance than F-RC at 3,000

samples. The trend in Figure 7(C) is similar to that in Figure 7(B), which is not too surprising since VE measures the contribution of the variance to the error rate. Interestingly, although RF has noticeably more variance at 500 samples than do Lumberjack and F-RC, it has slightly lower VE. It is also surprising that the VE of RF increases from 500 to 1000 training samples. In Figure 7(D), the error rate is shown for reference, which is the sum of bias and VE. Overall, these results suggest that Lumberjack wins on the sparse parity problem with a small sample size primarily through lower bias/SE, while with a larger sample size it wins mainly via lower variance/VE. A similar trend holds for the orthant problem (not shown).

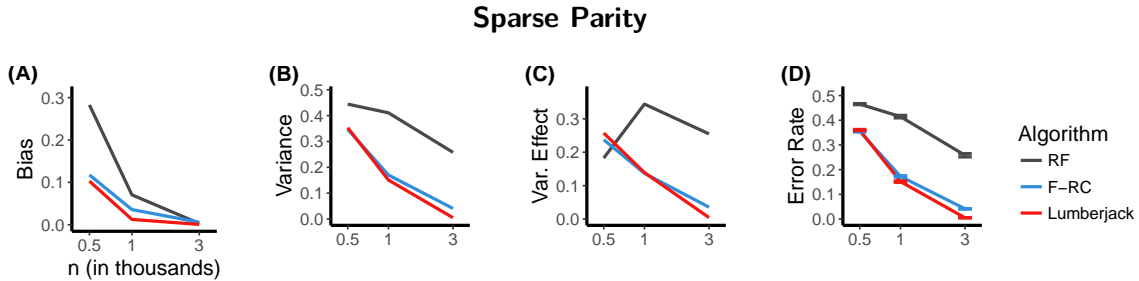


Figure 7: **(A-D)** Bias, variance, variance effect, and error rate, respectively, on the sparse parity problem as a function of the number of training samples. Error rate is the sum of systematic effect and variance effect, which roughly measure the contributions of bias and variance to the error rate, respectively. In this example, bias and systematic effect are identical because the Bayes error is zero (refer to [James, 2003]). For smaller training sets, Lumberjack wins primarily through lower bias/systematic effect, while for larger training sets it wins primarily through lower variance effect.

5.5 Lumberjack Provides Feature Importance

For many data scientists and researchers, understanding the observed data is just as critical as finding an algorithm with excellent predictive performance. One of the reasons for RF's popularity is its ability to learn good predictive models that simultaneously lend themselves to extraction of suitable feature importance measures. One such measure is the Gini importance [Breiman, 2001]. For a particular feature, it is defined as the sum of the reduction in Gini impurity over all splits of all trees made on that feature. With this metric, features that tend to yield splits with relatively pure nodes will have large importance scores. When using RF, features with low marginal information about the class label, but high pairwise or other higher-order joint distributional information, will likely receive relatively low importance scores. Since splits in Lumberjack are linear combinations of the original features, such features have a better chance of being identified. For Lumberjack, we compute Gini importance for each unique subspace. Of note, two vector projections that differ only by a sign are the same subspace.

Gini importance is computed for each feature on both RF and Lumberjack on the Trunk problem with $n = 1,000$. Figure 8(A,B) depict the linear weights of the observed features that define each of the top ten split node projections. Projections are sorted from highest Gini importance to lowest Gini importance. The top ten projections in Lumberjack are all linear combinations of dimensions, whereas in RF the projections can only be along single dimensions. RF fails to sort some of the individual features according to their "true" informativeness, where

true informativeness is measured by the Bayes error of a distribution along a projection. For example, RF ranks a projection along the ninth dimension as third most important. However, the dimensions are monotonically decreasing in importance, so it is actually the ninth most informative projection when only considering axis-aligned projections. The linear combinations in Lumberjack tend to include the first few dimensions, which contain most of the "true" signal. The best possible projection that Lumberjack could sample is the vector of all ones. However, since $\lambda = 1/2$ for this experiment, the probability of sampling such a dense projection having the appropriate coefficients is almost negligible. Figure 8(C) shows the normalized Gini importance of the top ten projections for each algorithm. Of top-10 most important features according to Lumberjack, they are all more important (in terms of Gini) than any of the RF features, except the very first one. Figure 8(D) shows the Bayes error rate of the top ten projections for each algorithm. Again, the majority of features Lumberjack selects are more informative than any of the ones that RF selects, except the very first.

6 Theoretical Analysis of Random Projection Forests

Let h_n denote a classifier learned from the training set D_n , and let L^* be the Bayes error rate. The sequence of classifiers h_n is consistent for a certain distribution f_{XY} if and only if $L(h_n) \rightarrow L^*$ as $n \rightarrow \infty$, and universally consistent if and only if h_n is consistent for all possible distributions f_{XY} .

Consistency theorems for the original RF procedure are extremely challenging to establish due to the combination of bagging and the greedy data-dependent nature of the split selection procedure, both of which are components of any RPF. To render theoretical analysis of RFs more tractable, analysis is often done on a simplified version of the RF procedure. In the same vein, we establish universal consistency of a simplified data-agnostic random projection forest procedure.

Definition 1. *The data-agnostic RPF is defined as the original random projection forest whose partition is random and independent of the class labels, that is, the split algorithm 2 is replaced by any random split mechanism that is independent of the class labels, and the projection matrix A is also sampled independently from the class labels.*

Theorem 2. *Denote the number of partitions of a random projection decision tree as t_n . Then data-agnostic RPF is universally consistent for classification when $t_n \rightarrow \infty$ and $t_n/n \rightarrow 0$ as $n \rightarrow \infty$.*

The universal consistency of data-agnostic RPF follows from Stone's theorem for local averaging estimates [Stone, 1977; Biau *et al.*, 2008].

Proof. This theorem essentially follows from Theorem 3.1 in Biau *et al.* [2008] by incorporating the random projection matrix: by Theorem 6.1 [Devroye *et al.*, 1996], data-agnostic RPF (or any partition algorithm that is independent of the class label) is consistent if $\text{diam}(B_n(X)) \rightarrow 0$ and $N_n(X) \rightarrow \infty$, where $B_n(X)$ is the random partition (the child node of RPF) that contains X , and

$$N_n(X) = \sum_{i=1}^n \mathbf{I}(X_i \in B_n(X))$$

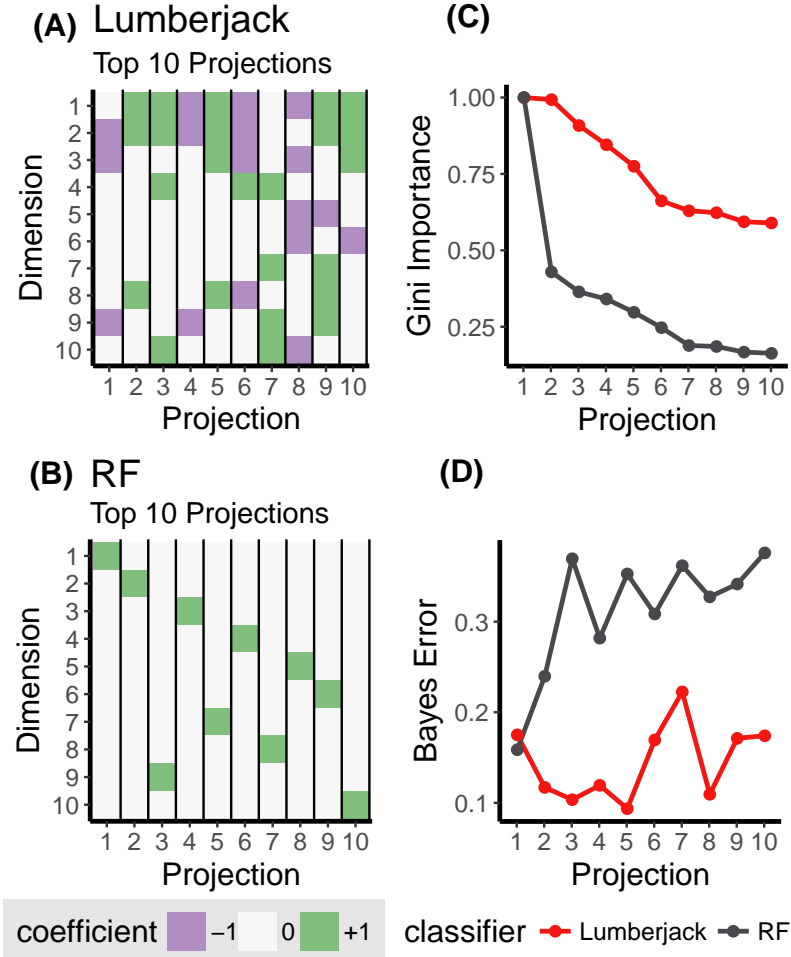


Figure 8: The ten projections with the highest Gini importance found by RF and Lumberjack on the Trunk problem with $p = 10, n = 1000$. **(A)** Visual representation of the top 10 projections identified by Lumberjack. The x-axis indicates the projection. The y-axis indicates the index of the ten canonical dimensions. The colors in the heat map indicate the linear coefficients of each canonical dimension that define each of the projections. **(B)** The same as (A), except for RF. **(C)** Comparison of the Gini importances of the 10 best projections found by each algorithm. **(D)** Comparison of the Bayes error of the 10 best projections found by each algorithm. The top 10 projections used in Lumberjack all have substantially lower Bayes error than those used in RF.

is the number of data points in the same partition as X , i.e., the number of training data in the same child node as X . Following the same step in Biau *et al.* [2008], any random partition algorithm satisfies

$$Prob(N_n(X) < t) \leq (t-1)t_n/(n+1) \rightarrow 0$$

for any fixed $t > 0$ when $t_n/(n+1) \rightarrow 0$. Thus $N_n(X) \rightarrow \infty$, and it remains to show that the diameter of $B_n(X)$ converges to 0 in probability.

As $t_n \rightarrow \infty$, the number of partitions for each dimension of $B_n(X)$ increases to ∞ , and since the partitions of data-agnostic RPF are randomly chosen for each dimension up to a

random projection, the size of each dimension of $B_n(X)$ is guaranteed to converge to 0 in probability. Therefore classification consistency holds for data-agnostic RPF. \square

Although we do not yet have a proof of the consistency of the data-adaptive and supervised RPFs, we do have a conjecture that some of these forests are “more” consistent than Breiman’s original RF. Biau *et al.* [2008] proposed a distribution for which Breiman’s RF is inconsistent. The joint distribution of (X, Y) is as follows: X has a uniform distribution on $[0, 1] \times [0, 1] \cup [1, 2] \times [1, 2] \cup [2, 3] \times [2, 3]$. Y is a deterministic function of X , that is $f(X) \in \{0, 1\}$. The $[0, 1] \times [0, 1]$ square is divided into countably infinite vertical stripes, and $[2, 3] \times [2, 3]$ square is similarly divided into countably infinite horizontal stripes. In both squares, the stripes with $f(X) = 0$ and $f(X) = 1$ alternate. The $[1, 2] \times [1, 2]$ square is a 2×2 checker board. Figure 9(A) shows a schematic illustration (because we cannot show countably infinite rows or columns). On this problem, Biau *et al.* [2008] show that RF cannot achieve an error lower than $1/6$. This is because RF will always choose to split either in the lower left square or top right square and never in the center square. On the other hand, Figure 9(B) shows that Lumberjack achieves effectively zero error. This is because although it is also greedy, with some probability it will choose oblique splits, that split the middle square to enable lower error. This suggests that Lumberjack is more consistent than RF.

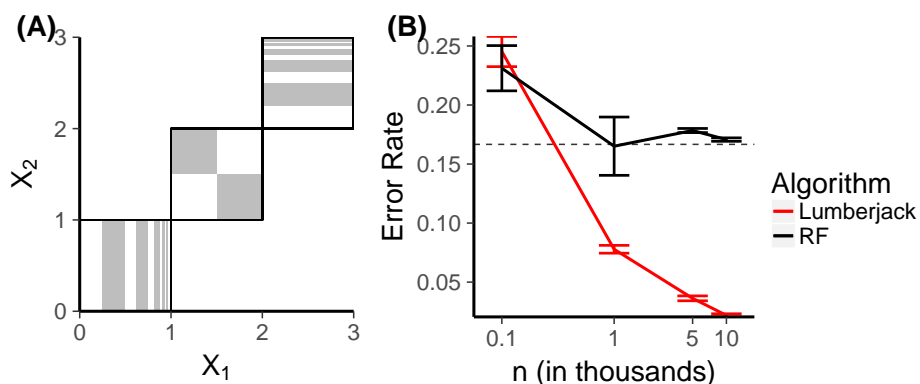


Figure 9: Classification performance on the consistency ($p = 2$) problem for various numbers of training samples. The consistency problem is designed such that RF has a theoretical lower bound of error of $1/6$. **(A)** The joint distribution of (X, Y) . X is uniformly distributed in the three unit squares. The lower left and upper right squares have countably infinite stripes, and the center square is a 2×2 checkerboard. The white areas represent $f(X) = 0$ and gray areas represent $f(X) = 1$. **(B)** Error rate as a function of n . The dashed line represents the lower bound of error for RF, which is $1/6$. Lumberjack performs better than RF, and the error rate empirically decreases to zero as n increases.

7 Computational Efficiency and Scalability of Lumberjack

7.1 Theoretical Time Complexity

The time complexity of an algorithm characterizes how the theoretical processing time for a given input relies on both the hyper-parameters of the algorithm and the characteristics of the input. Let T be the number of trees, n the number of training samples, p the number of features

in the training data, and d the number of features sampled at each split node. The average case time complexity of constructing a RF is $\mathcal{O}(Tdn \log^2 n)$ [Louppe, 2014]. The $dn \log n$ accounts for the sorting of d features at each node. The additional $\log n$ accounts for both the reduction in node size at lower levels of the tree and the average number of nodes produced. RF's near linear complexity shows that a good implementation will scale nicely with large input sizes, making it a suitable algorithm to process big data. Lumberjack's average case time complexity is similar to RF's, the only difference being the addition of a term representing a sparse matrix multiplication which is required in each node. This makes Lumberjack's complexity $\mathcal{O}(Td \log n(n \log n + \lambda p))$, where λ is the fraction of nonzeros in the $p \times d$ random projection matrix. We generally let λ be close to $1/p$, giving a complexity of $\mathcal{O}(Tdn \log^2 n)$, which is the same as for RF. Of note, in RF d is constrained to be no greater than p , the dimensionality of the data. Lumberjack, on the other hand, does not have this restriction on d . Therefore, if d is selected to be greater than p , Lumberjack may take longer to train. However, $d > p$ often results in improved classification performance.

7.2 Theoretical Space Complexity

The space complexity of an algorithm describes how the theoretical maximum memory usage during runtime scales with the inputs and hyperparameters. Let c be the number of classes and T , p , and n be defined as in Section 7.1. Building a single tree requires the data matrix to be kept in memory, which is $\mathcal{O}(np)$. During an attempt to split a node, two c -length arrays store the counts of each class to the left and to the right of the candidate split point. These arrays are used to evaluate the decrease in Gini impurity or entropy. Additionally, a series of random sparse projection vectors are sequentially assessed. Each vector has less than p nonzeros. Therefore this term is dominated by the np term. Assuming trees are fully grown, meaning each leaf node contains a single data point, the tree has $2n$ nodes in total. This term gets dominated by the np term as well. Therefore, the space complexity to build a Lumberjack is $\mathcal{O}(T(np + c))$. This is the same as that of RFs.

7.3 Theoretical Storage Complexity

We define storage complexity as the dependency of disk space required to store a forest on the inputs and hyperparameters. Assume that trees are fully grown. For each leaf node, only the class label of the training data point contained within the node is stored, which is $\mathcal{O}(1)$. For each split node, the split dimension index and threshold are stored, which are also both $\mathcal{O}(1)$. Therefore, the storage complexity of a RF is $\mathcal{O}(Tn)$.

For a Lumberjack, the only aspect that differs is that a (sparse) vector projection along which to split is stored at each split node rather than a single split dimension index. Let z denote the number of nonzero entries in a vector projection stored at each split node. Storage of this vector at each split node requires $\mathcal{O}(z)$ memory. Therefore the storage complexity of a Lumberjack is $\mathcal{O}(Tnz)$. z is a random variable whose prior is governed by λ , which is typically set to $1/p$. The posterior mean of z is determined also by the data; empirically it is close to $z = 1$. Therefore, in practice, the storage complexity of Lumberjack is close to that of RF.

7.4 Empirical Speed and Scalability

7.4.1 Comparison of Algorithms Using the Same Implementation

Figure 10(A) shows the training times of RF, F-RC, and Lumberjack on the sparse parity problem. Training times reported are those corresponding to the best hyperparameter settings for each algorithm. Experiments are run using an Intel Xeon E5-2650 v3 processors clocked at 2.30GHz with 10 physical cores and 20 threads and 250 GB DDR4-2133 RAM. The operating system is Ubuntu 16.04. F-RC is the slowest, RF is the fastest, and Lumberjack is in between. While not shown, we note that a similar trend holds for the orthant problem. Figure 10(B) shows that when the hyperparameter d of Lumberjack and F-RC is the same as that for RF, training times are comparable. However, training time continues to increase as d exceeds p for Lumberjack and F-RC, which largely accounts for the trend seen in Figure 10(A). Figure 10(C) indicates that this additional training time comes with the benefit of substantially improved accuracy. Restricting d to be no greater than p for Lumberjack in this setting would still perform noticeably better than RF at no additional cost in training time. Therefore, Lumberjack does not trade off accuracy for time, rather, for a fixed computational budget, it achieves better accuracy; and if allowed to use more computation, further improves accuracy.

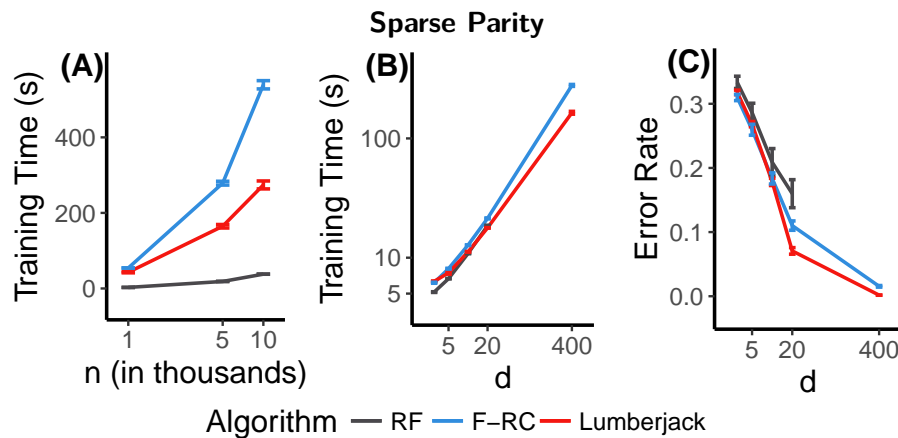


Figure 10: Comparison of training times of RF, Lumberjack, and F-RC on the 20-dimensional sparse parity data set. **(A)** Dependency of training time using the best set of hyperparameters (y-axis) on the number of training samples (x-axis) for the sparse parity problem. **(B)** Dependency of training time (y-axis) on the number of projections sampled at each split node (x-axis) for the sparse parity problem with $n = 5,000$. **(C)** Dependency of error rate (y-axis) on the number of projections sampled at each split node (x-axis) for the sparse parity problem with $n = 5,000$. Lumberjack and F-RC can sample many more than p projections, unlike RF. As seen in panels (B) and (C), doing so dramatically improves classification performance at the expense of larger training times. However, comparing error rates and training times at $d = 20$, Lumberjack can classify substantially better than RF even with no additional cost in training time.

7.4.2 Comparison of Different Implementations

We developed and maintain an open multi-core R implementation of Lumberjack which is hosted on CRAN [Browne *et al.*, 2018a]. We compare speed of training and strong scaling of our implementation to those of the R Ranger [Wright, 2018] and XGBoost [Chen, 2018]

packages, which are currently two of the fastest parallelized decision tree ensemble software packages available. Ranger offers a fast multicore version of RF that has been extensively optimized for runtime performance. XGBoost offers a fast multicore version of gradient boosted trees, and computational performance is optimized for shallow trees. Both Ranger and XGBoost are C++ implementations with R wrappers, whereas our Lumberjack implementation is almost entirely native R. Strong scaling is the relative increase in speed of using multiple cores over that of using a single core. In the ideal case, the use of N cores would produce a factor N speedup. Hyperparameters are chosen for each implementation so as to make the comparisons fair. For all implementations, trees are grown to full depth, 100 trees are constructed, and $d = \sqrt{p}$ features sampled at each node. For Lumberjack, $\lambda = 1/p$. Experiments are run using four Intel Xeon E7-4860 v2 processors clocked at 2.60GHz, each processor having 12 physical cores and 24 threads. The amount of available memory is 1 TB DDR3-1600. The operating system is Ubuntu 16.04. Comparisons use three openly available large data sets:

MNIST The MNIST data set [Lecun *et al.*] has 60,000 training observations and 784 (28x28) features. In Figure 11(A), for a small number of cores, Lumberjack is faster than XGBoost but slower than Ranger. However, when 48 cores are used, Lumberjack is as fast as Ranger and still faster than XGBoost. Figure 11(D) shows that Lumberjack has the best strong scaling for this data set.

Higgs The Higgs data set (<https://www.kaggle.com/c/higgs-boson>) has 250,000 training observations and 31 features. Figure 11(B) shows that when 48 cores are used, Lumberjack is as fast as ranger and faster than XGBoost. Figure 11(E) again shows that Lumberjack utilizes additional cores more effectively than the other implementations.

p53 The p53 data set (<https://archive.ics.uci.edu/ml/datasets/p53+Mutants>) has 31,159 training observations and 5,409 features. Figure 11(C) shows a similar trend as for MNIST. Figure 11(F) indicates that Lumberjack has strong scaling in between that of Ranger and XGBoost. For this data set, utilizing additional resources with Lumberjack does not provide as much benefit due to the classification task being too easy (all algorithms achieve perfect classification accuracy)—the trees are shallow, causing the overhead cost of multithreading to outweigh the speed increase due to parallelism.

We also compare prediction times of the various implementations on the same three data sets (Figure 12). In addition to our standard Lumberjack prediction implementation, we also compare our "Forest Packing" prediction implementation. The number of test points used for the Higgs, MNIST, and p53 data sets is 50,000, 10,000, and 6,000, respectively. Predictions were made sequentially without batching using a single core. Lumberjack is significantly faster than Ranger on the Higgs and MNIST data sets, and only marginally slower on the p53 data set. XGBoost is much faster than both Lumberjack and Ranger, which is due to the fact that the XGBoost algorithm constructs much shallower trees than the other methods. Most notably, the Forest Packing procedure, which "packs" the trees learned by Lumberjack, makes predictions roughly ten times faster than XGBoost and over 100 times faster than the standard Lumberjack on all three data sets.

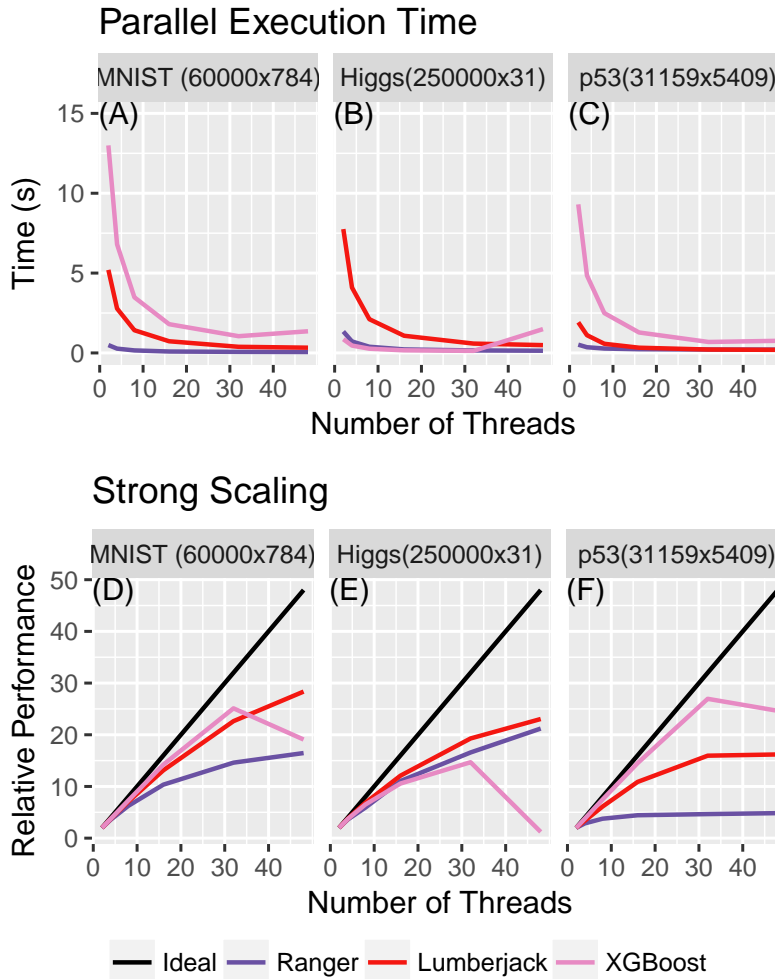


Figure 11: **(A-C)** The per tree training time for three large real world data sets. Training was performed using matching parameters where possible and default parameters otherwise. Lumberjack’s performance is comparable to the highly optimized XGBoost and Ranger and even outperforms XGBoost on two of the data sets. **(D-F)**: Strong scaling is the time needed to train a forest with one core divided by the time needed to train a forest with multiple cores. This is a measurement of a system’s ability to efficiently utilize additional resources. Lumberjack is able to scale well over the entire range of tested cores whereas XGBoost has sharp drops in scalability where it is unable to use additional threads due to characteristics of the given data sets. The p53 data set, despite having a large number of dimensions, is easily classifiable, which leads to short trees. The p53 strong scaling plot shows that when trees are short the overhead of multithreading prevents Lumberjack from efficiently using the additional resources.

8 Structured Lumberjack

Another compelling feature of RPF is that a projection distribution can be chosen to exploit domain knowledge. We consider two additional examples, where the data do not live in p -dimensional Euclidean space, but rather image space and a circle. In each case, we design

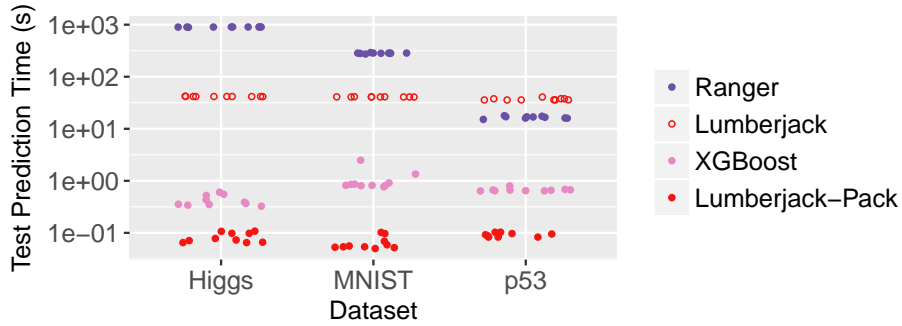


Figure 12: Comparison of test set prediction times. Forest Packing results show a 10x speed up in real time prediction scenarios. Test set sizes: Higgs, 50,000 observations; MNIST, 10,000 observations; p53, 6,000 observations. Predictions were made sequentially without batching.

a projection distribution appropriate for the space, and demonstrate dramatically improved performance.

In computer vision tasks, good features are typically ones that exploit the spatial relationship of pixels within images. These features can be manually engineered using expert domain knowledge or they can be learned using deep learning methods such as convolutional neural networks (CNNs). In a similar vein, we propose a projection distribution which enables the learning procedure to exploit spatial structure. We will refer to this particular variant of Lumberjack as Structured Lumberjack (S-Lumberjack). At each split node, S-Lumberjack randomly samples d rectangular patches of spatially contiguous pixels. Patch heights and widths are sampled uniformly at random and independent of each other. Patch locations are sampled uniformly at random. For each patch, a new feature is constructed by summing the intensities of the pixels within the patch.³ The split is made by optimizing the split criterion over this set of d constructed features. The key idea here is that by constructing new features from spatially contiguous pixels, the features can represent low-level objects like simple edges and shapes. These low-level objects can then be used to construct meaningful hierarchical decision rules using a dictionary of patches (rather than pixels). To test this idea, we constructed a toy image classification problem. One class of images contains randomly sized and spaced horizontal lines. The other class contains randomly sized and spaced vertical lines. The probability distributions of the images are identical if a 90 degree rotation is applied to one of the classes. Figure 13(A) shows three example images from each class. Figure 13(B) shows performance of RF, the default Lumberjack, S-Lumberjack, and a control Lumberjack. The control Lumberjack samples pixels with the same distribution and parameters as S-Lumberjack, but ignoring spatial contiguity. S-Lumberjack shows significant improvement in classification performance over all other algorithms.

The second non-Euclidean example, inspired by [Younes, 2018], is a two class classification problem in which each data point is a discretization of the unit circle into 100 points with two embedded sequences of 1's in two differing patterns: class 1 has two sequences of length 5 and class 2 has two sequences of length 4 and 6 (not respective of order). Here, the projection distribution consists of continuous one-dimensional patches, rather than two dimensional as for

³In general, the pixel intensities can be weighted when summing.

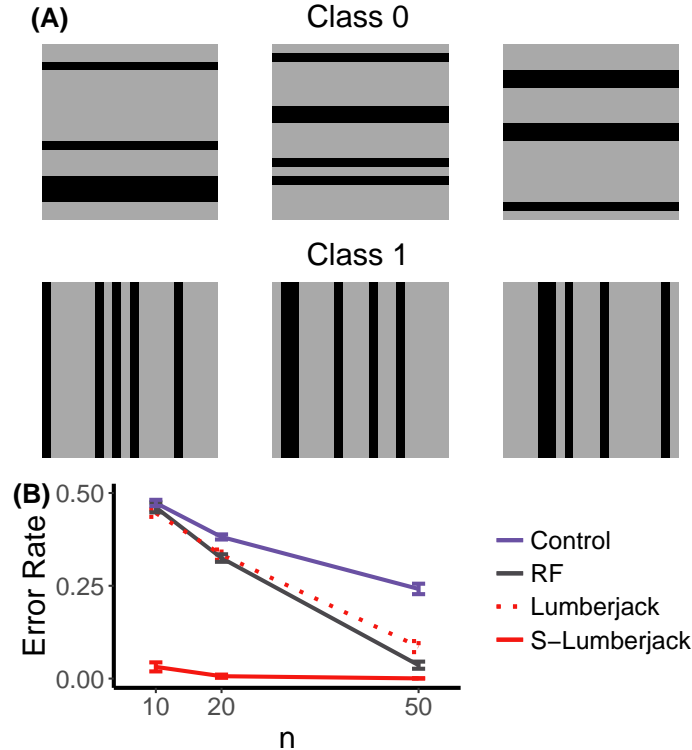


Figure 13: Exploiting spatial structure in image classification. **(A)** Simulated images: Class 0 are horizontal bars; Class 1 are vertical bars. **(B)**: classification performance of Structure Lumberjack (S-Lumberjack), Lumberjack, RF, and Control Lumberjack (using the same projection sparsity as that in Structure Lumberjack), demonstrates that S-Lumberjack achieves a dramatic empirical improvement in efficiency.

the images. Moreover, the projection distribution respects the nonlinear manifold, meaning that projections “wrap-around” the dimensions to ensure they are always contiguous. In this setting, S-Lumberjack has the same two parameters as typical Lumberjack: number of features and expected density. Like the image data, we sample uniform numbers between 0 and 1 for each selected dimension. As compared with RF, as well as several other standard machine learning algorithms, S-Lumberjack performs dramatically better, with only a multi-layer perceptron achieving the same error rates.

9 Discussion

RPF provides a general framework that encapsulates many orthogonal and oblique tree ensemble methods. Our open-source implementation allows users to easily specify any projection distribution they desire.

The RPF framework opens up a myriad of paths to explore. On the theoretical side, the theorems in Biau *et al.* [2016] for RF can be immediately extended to RPFs with some minor modifications—their proofs rely on clever adaptations of classical consistency results for data-independent partitioning classifiers, which are agnostic to whether the partitions are hyper-rectangular or not. Moreover, we hope that theoretical investigations will yield more insight into

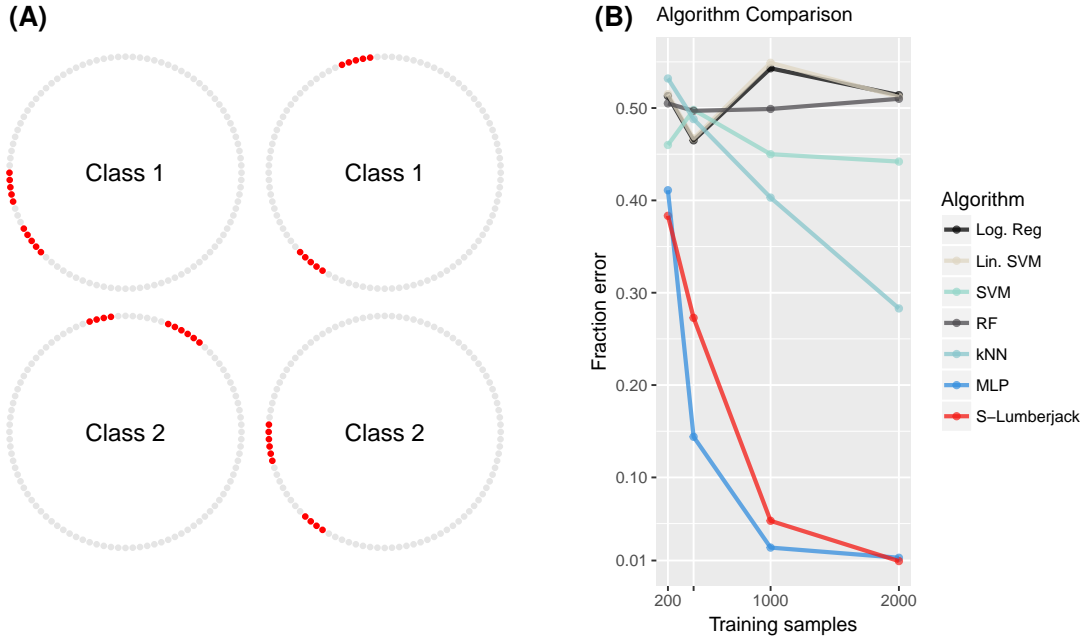


Figure 14: **(A)**: A sample of the toy data. **(B)**: Data for the Logistic Regression (Log. Reg.), Linear SVM (Lin. SVM), SVM, Random Forest (RF), k -Nearest Neighbors, and Multi-layer Perceptrons (MLP) were obtained from §8.5 Table 5 in [Younes, 2018]. The data for S-Rerf were obtained by our own experiment with the setup as described in §8.5 of Younes [2018].

which projection distribution will be optimal under different distributional settings, both asymptotically and under finite sample assumptions. For instance, Biau *et al.* [2008] construct a distribution for which RF with fixed depth is guaranteed to have a probability of error of at least $1/6$. Although the optimal decision boundary is a union of axis-aligned splits, the greedy nature in which splits are selected (rather than global optimization) prevents it from learning the appropriate rules, regardless of the amount of training data. Lumberjack achieves a probability of error indistinguishable from zero on this problem, probably because it is less greedy [Meinshausen, 2006]. The idea that certain oblique methods are consistent on a wider class of problems seems plausible. Additionally, it would be interesting to see what theoretical guarantees hold when the projection distribution depends on the data. In other words, when a supervised procedure is used to identify (hopefully) strong discriminant directions, are there different/additional conditions needed to guarantee consistency? Since such procedures may substantially reduce the diversity of trees, it seems plausible that the data subsampling and/or depth conditions required for consistency in Biau *et al.* [2016] may need to be adjusted. Indeed, Rainforth and Wood [2015] suggests that in order to achieve strong empirical performance, their novel projection bootstrapping procedure in place of the typical bagging procedure is often helpful.

Another avenue is to further explore Structured Lumberjack, in computer vision as well as in other domains. In this work we only present one probability distribution on random projection matrices for exploiting spatial structure for computer vision. Furthermore, our image classification example is a rudimentary and artificial toy problem which does not impose many of the challenges that real-world image classification problems have. Nonetheless, the point was simply to illustrate how domain knowledge can be used to bias the sampling distribution in order to

achieve better performance. As a final statement, we vouch that our RPF implementation is a competitive alternative to existing tree ensemble implementations, and can in fact realize many previously proposed tree ensemble methods, possibly with some minor modifications. Open source code is available: <https://github.com/neurodata/R-RerF> and from CRAN.

Acknowledgments

This work is graciously supported by the Defense Advanced Research Projects Agency (DARPA) SIMPLEX program through SPAWAR contract N66001-15-C-4041 and DARPA GRAPHS N66001-14-1-4028.

References

- Dimitris Achlioptas. Database-friendly random projections: Johnson-lindenstrauss with binary coins. *Journal of computer and System Sciences*, 66(4):671–687, 2003.
- G. Biau, L. Devroye, and G. Lugosi. Consistency of random forests and other averaging classifiers. *The Journal of Machine Learning Research*, 9:2015–2033, 2008.
- G erard Biau, Erwan Scornet, and Johannes Welbl. Neural random forests. *arXiv preprint arXiv:1604.07143*, 2016.
- Ella Bingham and Heikki Mannila. Random projection in dimensionality reduction: applications to image and text data. In *Proceedings of the seventh ACM SIGKDD international conference on Knowledge discovery and data mining*, pages 245–250. ACM, 2001.
- Rico Blaser and Piotr Fryzlewicz. Random rotation ensembles. *Journal of Machine Learning Research*, 17(4):1–26, 2016.
- Leo Breiman et al. Arcing classifier (with discussion and a rejoinder by the author). *The annals of statistics*, 26(3):801–849, 1998.
- L. Breiman. Random forests. *Machine Learning*, 4(1):5–32, October 2001.
- James Browne, Tyler Tomita, and Joshua T. Vogelstein. *ref: Randomer Forest*, 2018.
- James Browne, Tyler M Tomita, Disa Mhembere, Randal Burns, and Joshua T Vogelstein. Forest packing: Fast, parallel decision forests. June 2018.
- Rich Caruana and Alexandru Niculescu-Mizil. An empirical comparison of supervised learning algorithms. In *Proceedings of the 23rd international conference on Machine learning*, pages 161–168. ACM, 2006.
- R. Caruana, N. Karampatziakis, and A. Yessenalina. An empirical evaluation of supervised learning in high dimensions. *Proceedings of the 25th International Conference on Machine Learning*, 2008.
- Tianqi Chen and Carlos Guestrin. Xgboost: A scalable tree boosting system. In *Proceedings of the 22nd acm sigkdd international conference on knowledge discovery and data mining*, pages 785–794. ACM, 2016.
- Tianqi Chen. *xgboost: Extreme Gradient Boosting*, 2018.
- Sanjoy Dasgupta and Yoav Freund. Random projection trees and low dimensional manifolds. In *Proceedings of the Fortieth Annual ACM Symposium on Theory of Computing*, STOC '08, pages 537–546, New York, NY, USA, 2008. ACM.

- S Dasgupta and Y Freund. Random projection trees for vector quantization. *IEEE Transactions on Information*, 2009.
- S Dasgupta and K Sinha. Randomized partition trees for exact nearest neighbor search. *Conference on Learning Theory*, 2013.
- L. Devroye, L. Gyorfi, and G. Lugosi. *A Probabilistic Theory of Pattern Recognition*. 1996.
- Dirk Eddebuettel. *Rcpp: Seamless R and C++ Integration*, 2018.
- Xiaoli Z Fern and Carla E Brodley. Random projection for high dimensional data clustering: A cluster ensemble approach. In *Proceedings of the 20th international conference on machine learning (ICML-03)*, pages 186–193, 2003.
- M. Fernandez-Delgado, E. Cernadas, S. Barro, and D. Amorim. Do we need hundreds of classifiers to solve real world classification problems? *Journal of Machine Learning Research*, 15(1):3133–3181, October 2014.
- Dmitriy Fradkin and David Madigan. Experiments with random projections for machine learning. In *Proceedings of the ninth ACM SIGKDD international conference on Knowledge discovery and data mining*, pages 517–522. ACM, 2003.
- Jerome H Friedman. Greedy function approximation: a gradient boosting machine. *Annals of statistics*, pages 1189–1232, 2001.
- D. Heath, S. Kasif, and S. Salzberg. Induction of oblique decision trees. *Journal of Artificial Intelligence Research*, 2(2):1–32, 1993.
- Chinmay Hegde, Michael Wakin, and Richard Baraniuk. Random projections for manifold learning. In *Advances in neural information processing systems*, pages 641–648, 2008.
- Gareth M James. Variance and bias for general loss functions. *Machine Learning*, 51(2):115–135, 2003.
- Guolin Ke, Qi Meng, Thomas Finley, Taifeng Wang, Wei Chen, Weidong Ma, Qiwei Ye, and Tie-Yan Liu. Lightgbm: A highly efficient gradient boosting decision tree. In I. Guyon, U. V. Luxburg, S. Bengio, H. Wallach, R. Fergus, S. Vishwanathan, and R. Garnett, editors, *Advances in Neural Information Processing Systems 30*, pages 3146–3154. Curran Associates, Inc., 2017.
- Yann Lecun, Corinna Cortes, and Christopher J.C. Burges. *The MNIST Database of Handwritten Digits*.
- P. Li, T. J. Hastie, and K. W. Church. Very sparse random projections. In *Proceedings of the 12th ACM SIGKDD international conference on Knowledge discovery and data mining*, pages 287–296. ACM, 2006.
- Gilles Louppe. Understanding random forests: From theory to practice. *arXiv preprint arXiv:1407.7502*, 2014.
- Nicolai Meinshausen. Quantile regression forests. *J. Mach. Learn. Res.*, 7(Jun):983–999, 2006.

- B. H. Menze, B.M Kelm, D. N. Splitthoff, U. Koethe, and F. A. Hamprecht. On oblique random forests. In Dimitrios Gunopulos, Thomas Hofmann, Donato Malerba, and Michalis Vazirgiannis, editors, *Machine Learning and Knowledge Discovery in Databases*, volume 6912 of *Lecture Notes in Computer Science*, pages 453–469. Springer Berlin Heidelberg, 2011.
- Tom Rainforth and Frank Wood. Canonical correlation forests. *arXiv preprint arXiv:1507.05444*, 2015.
- J. J. Rodriguez, L. I. Kuncheva, and C. J. Alonso. Rotation forest: A new classifier ensemble method. *Pattern Analysis and Machine Intelligence, IEEE Transactions on*, 28(10):1619–1630, 2006.
- Robert E Schapire. The strength of weak learnability. *Mach. Learn.*, 5(2):197–227, July 1990.
- Charles J Stone. Consistent nonparametric regression. *The annals of statistics*, pages 595–620, 1977.
- Tyler M Tomita, Mauro Maggioni, and Joshua T Vogelstein. Roflmao: Robust oblique forests with linear matrix operations. In *SIAM Data Mining*, 2017.
- G. V. Trunk. A problem of dimensionality: A simple example. *Pattern Analysis and Machine Intelligence, IEEE Transactions on*, (3):306–307, 1979.
- Roman Vershynin. *High Dimensional Probability: An Introduction with Applications in Data Science*. 2017.
- Marvin N. Wright. *ranger: A fast Implementation of Random Forests*, 2018.
- A J Wyner, M Olson, J Bleich, and D Mease. Explaining the success of adaboost and random forests as interpolating classifiers. *J. Mach. Learn. Res.*, 2017.
- Laurent Younes. Diffeomorphic Learning. *arXiv preprint arXiv:1806.01240*, 2018.

A Hyperparameter Tuning

Hyperparameters in XGBoost are tuned via grid search using the R caret package. The values tried for each hyperparameter are based on suggestions by Owen Zhang (<https://www.slideshare.net/OwenZhang2/tips-for-data-science-competitions>), a research data scientist who has had many successes in data science competitions using XGBoost:

- nrounds: 100, 1000
- subsample: 0.5, 0.75, 1
- eta: 0.001, 0.01
- colsample_bytree: 0.4, 0.6, 0.8, 1
- min_child_weight: 1
- max_depth: 4, 6, 8, 10, 100000

- gamma: 0

Selection of the hyperparameter values is based on minimization of a five-fold cross-validation error rate.

B Real Benchmark data sets

B.1 Classification

We use 105 benchmark data sets from the UCI machine learning repository for classification. These data sets are most of the data sets used in Fernandez-Delgado *et al.* [2014]; some were removed due to licensing or unavailability issues. We noticed certain anomalies in Fernandez-Delgado *et al.* [2014]’s pre-processed data, so we pre-processed the raw data again as follows.

1. **Remove of nonsensical features.** Some features, such as unique sample identifiers, or features that were the same value for every sample, were removed.
2. **Imputate missing values.** The R randomForest package was used to impute missing values. This method was chosen because it is nonparametric and is one of the few imputation methods that can natively impute missing categorical entries.
3. **One-hot-encode categorical features.** Most classifiers cannot handle categorical data natively. Given a categorical feature with possible values $\{C_1, \dots, C_m\}$, we expand to m binary features. If a data point has categorical value $C_k, \forall k \in 1, \dots, m$ then the k th binary feature is assigned a value of one and zero otherwise.
4. **Integer encoding of ordinal features.** Categorical features having order to them, such as "cold", "luke-warm", and "hot", were numerically encoded to respect this ordering with integers starting from 1.
5. **Standardization of the format.** Lastly, all data sets were stored as CSV files, with rows representing observations and columns representing features. The class labels were placed as the last column.
6. **Five-fold partition.** Each data set was randomly divided into five partitions for five-fold cross-validation. Partitions preserved the relative class frequencies by stratification.

B.2 Regression

For regression, RF, Lumberjack, and CCF are compared on 42 out of the 61 data sets from the WEKA data set collection⁴. These data sets were taken from [Rainforth and Wood, 2015]’s GitHub repository⁵. We performed the same preprocessing steps from Section 3.3 of Rainforth as follows (some of the preprocessing was already done in the downloaded data set):

1. **One-hot-encoding categorical features.**
2. **Standardization of features.** Each feature was standardized across all samples (excluding missing features) to have 0 mean and unit variance.
3. **Missing value sampling.** Missing values were replaced with a random sample from $N(0, 1)$.
4. **Standardization of the format.**
5. **Five-fold partitioning.**

⁴[https://www.cs.waikato.ac.nz/ml/weka/data sets.html](https://www.cs.waikato.ac.nz/ml/weka/data%20sets.html)

⁵[https://github.com/twgr/ccfs/tree/master/data sets/regression](https://github.com/twgr/ccfs/tree/master/data%20sets/regression)

19 out of the 61 data sets were not included in Rainforth's GitHub repository due to licensing issues, so we excluded them from our analysis.

C Pseudocodes

Pseudocode 1 Learning a Random Projection Forest decision tree.

Input: (1) \mathcal{D}_n : training data (2) d : dimensionality of the projected space, (3) $f_{\mathbf{A}}$: distribution of the random projection matrix, (4) Θ : set of split eligibility criteria

Output: A RPF decision tree T

```

1: function  $T = \text{GROWTREE}(\mathbf{X}, \mathbf{y}, f_{\mathbf{A}}, \Theta)$ 
2:    $c = 1$  ▷  $c$  is the current node index
3:    $M = 1$  ▷  $M$  is the number of nodes currently existing
4:    $S^{(c)} = \text{bootstrap}(\{1, \dots, n\})$  ▷  $S^{(c)}$  is the indices of the observations at node  $c$ 
5:   while  $c < M + 1$  do ▷ visit each of the existing nodes
6:      $(\mathbf{X}', \mathbf{y}') = (\mathbf{x}_i, y_i)_{i \in S^{(c)}}$  ▷ data at the current node
7:     for  $k = 1, \dots, K$  do  $n_k^{(c)} = \sum_{i \in S^{(c)}} I[y_i = k]$  end for ▷ class counts (for classification)
8:     if  $\Theta$  satisfied then ▷ do we split this node?
9:        $\mathbf{A} = [\mathbf{a}_1 \cdots \mathbf{a}_d] \sim f_{\mathbf{A}}$  ▷ sample random  $p \times d$  matrix
10:       $\tilde{\mathbf{X}} = \mathbf{A}^T \mathbf{X}' = (\tilde{\mathbf{x}}_i)_{i \in S^{(c)}}$  ▷ random projection into new feature space
11:       $(j^*, t^*) = \text{findbestsplit}(\tilde{\mathbf{X}}, \mathbf{y}')$  ▷ Algorithm 2
12:       $S^{(M+1)} = \{i : \mathbf{a}_{j^*} \cdot \tilde{\mathbf{x}}_i \leq t^* \quad \forall i \in S^{(c)}\}$  ▷ assign to left child node
13:       $S^{(M+2)} = \{i : \mathbf{a}_{j^*} \cdot \tilde{\mathbf{x}}_i > t^* \quad \forall i \in S^{(c)}\}$  ▷ assign to right child node
14:       $\mathbf{a}^{*(c)} = \mathbf{a}_{j^*}$  ▷ store best projection for current node
15:       $\tau^{*(c)} = t^*$  ▷ store best split threshold for current node
16:       $\kappa^{(c)} = \{M + 1, M + 2\}$  ▷ node indices of children of current node
17:       $M = M + 2$  ▷ update the number of nodes that exist
18:     else
19:        $(\mathbf{a}^{*(c)}, \tau^{*(c)}, \kappa^{*(c)}) = \text{NULL}$ 
20:     end if
21:      $c = c + 1$  ▷ move to next node
22:   end while
23:   return  $(S^{(1)}, \{\mathbf{a}^{*(c)}, \tau^{*(c)}, \kappa^{(c)}\}_{c=1}^{m-1}, \{n_k^{(c)}\}_{k \in \mathcal{Y}}_{c=1}^{m-1})$ 
24: end function

```

Pseudocode 2 Finding the best node split. This function is called by growtree (Alg 1) at every split node. For each of the p dimensions in $\mathbf{X} \in \mathbb{R}^{p \times n}$, a binary split is assessed at each location between adjacent observations. The dimension j^* and split value τ^* in j^* that best split the data are selected. The notion of “best” means maximizing some choice in scoring function. In classification, the scoring function is typically the reduction in Gini impurity or entropy. The increment function called within this function updates the counts in the left and right partitions as the split is incrementally moved to the right.

Input: (1) $(\mathbf{X}, \mathbf{y}) \in \mathbb{R}^{p \times n} \times \mathcal{Y}^n$, where $\mathcal{Y} = \{1, \dots, K\}$

Output: (1) dimension j^* , (2) split value τ^*

```

1: function  $(j^*, \tau^*) = \text{FINDBESTSPPLIT}(\mathbf{X}, \mathbf{y})$ 
2:   for  $j = 1, \dots, p$  do
3:     Let  $\mathbf{x}^{(j)} = (x_1^{(j)}, \dots, x_n^{(j)})$  be the  $j$ th row of  $\mathbf{X}$ .
4:      $\{m_i^j\}_{i \in [n]} = \text{sort}(\mathbf{x}^{(j)})$  ▷  $m_i^j$  is the index of the  $i^{\text{th}}$  smallest value in  $\mathbf{x}^{(j)}$ 
5:      $t = 0$  ▷ initialize split to the left of all observations
6:      $n' = 0$  ▷ number of observations left of the current split
7:      $n'' = n$  ▷ number of observations right of the current split
8:     if (task is classification) then
9:       for  $k = 1, \dots, K$  do
10:         $n_k = \sum_{i=1}^n I[y_i = k]$  ▷ total number of observations in class  $k$ 
11:         $n'_k = 0$  ▷ number of observations in class  $k$  left of the current split
12:         $n''_k = n_k$  ▷ number of observations in class  $k$  right of the current split
13:       end for
14:     end if
15:     for  $t = 1, \dots, n - 1$  do ▷ assess split location, moving right one at a time
16:        $(\{n'_k, n''_k\}, n', n'', y_{m_t^j}) = \text{increment}(\{n'_k, n''_k\}, n', n'', y_{m_t^j})$ 
17:        $Q^{(j,t)} = \text{score}(\{n'_k, n''_k\}, n', n'')$  ▷ measure of split quality
18:     end for
19:   end for
20:    $(j^*, t^*) = \underset{j,t}{\text{argmax}} Q^{(j,t)}$ 
21:   for  $i = 0, 1$  do  $c_i = m_{t^*+i}^{j^*}$  end for
22:    $\tau^* = \frac{1}{2}(x_{c_0}^{(j^*)} + x_{c_1}^{(j^*)})$  ▷ compute the actual split location from the index  $j^*$ 
23:   return  $(j^*, \tau^*)$ 
24: end function

```

D Data Tables

Dataset	n	p_{num}	p_{cat}	5-fold CV Error Rate				
				Lumberjack	RF	XGBoost	RR-RF	CCF
abalone	4177	7	1	0.888 ± 0.019	0.89 ± 0.03	0.882 ± 0.03	0.909 ± 0.004	0.906 ± 0.009
acute_inflammation_task_1	120	6	0	0 ± 0.018	0 ± 0.1	0.05 ± 0.06	0 ± 0.003	0 ± 0.008
acute_inflammation_task_2	120	6	0	0 ± 0.009	0 ± 0.13	0.13 ± 0.05	0 ± 0.004	0 ± 0.011
adult	32561	7	7	0.1762 ± 0.012	0.1758 ± 0.15	0.1655 ± 0.07	0.2184 ± 0.18	0.1972 ± 0.01
annealing	798	27	5	0.02 ± 0.023	0.02 ± 0.07	0.03 ± 0.04	0.09 ± 0.06	0.06 ± 0.011
arrhythmia	452	279	0	0.28 ± 0	0.26 ± 0.11	0.28 ± 0.04	0.39 ± 0.19	0.34 ± 0.013
audiology_std	200	68	1	0.25 ± 0	0.27 ± 0	0.27 ± 0.04	0.35 ± 0.23	0.24 ± 0.012
balance_scale	625	4	0	0.06 ± 0.04	0.23 ± 0.02	0.17 ± 0.028	0.18 ± 0.14	0.1 ± 0.009
balloons	16	4	0	0.6 ± 0	0.5 ± 0.04	0.9 ± 0.035	0.4 ± 0.002	0.6 ± 0.012
bank	4521	11	5	0.083 ± 0	0.081 ± 0.01	0.081 ± 0.027	0.087 ± 0.002	$0.084 \pm 3e - 04$
blood	748	4	0	0.29 ± 0	0.28 ± 0.02	0.28 ± 0.031	0.29 ± 0.003	$0.3 \pm 3e - 04$
breast_cancer	286	7	2	0.39 ± 0	0.4 ± 0.063	0.42 ± 0.025	0.46 ± 0.001	$0.43 \pm 3e - 04$
breast_cancer-wisconsin	699	9	0	0.04 ± 0.19	0.04 ± 0.043	0.05 ± 0.5	0.04 ± 0.002	$0.04 \pm 3e - 04$
³⁸ breast_cancer-wisconsin-diag	569	30	0	0.04 ± 0	0.06 ± 0.039	0.06 ± 0.4	0.04 ± 0.1	$0.03 \pm 2e - 04$
breast_cancer-wisconsin-prog	198	33	0	0.27 ± 0	0.31 ± 0.031	0.28 ± 0.5	0.28 ± 0.09	0.28 ± 0.02
car	1728	6	0	0.035 ± 0.0065	0.069 ± 0.031	0.035 ± 0.3	0.185 ± 0.11	0.031 ± 0.04
cardiotocography_task_1	2126	21	0	0.165 ± 0.0064	0.175 ± 0.03	0.156 ± 0.4	0.253 ± 0.04	0.185 ± 0.03
cardiotocography_task_2	2126	21	0	0.061 ± 0.0063	0.064 ± 0.01	0.055 ± 0.0029	0.099 ± 0.08	0.077 ± 0.05
chess_krvk	28056	0	6	0.1599 ± 0.0087	0.2201 ± 0.03	0.1324 ± 0.0025	0.4083 ± 0.1	0.149 ± 0.01
chess_krvkp	3196	35	1	0.009 ± 0.0063	0.012 ± 0.04	0.012 ± 0.0011	0.043 ± 0.1	0.014 ± 0.023
congressional_voting	435	16	0	0.06 ± 0.02	0.06 ± 0.04	0.04 ± 0.0049	0.06 ± 0.12	0.06 ± 0.014
conn_bench-sonar-mines-rocks	208	60	0	0.28 ± 0.03	0.28 ± 0.03	0.23 ± 0.0037	0.3 ± 0.11	0.24 ± 0.021
conn_bench-vowel-deterding	528	11	0	0.03 ± 0.03	0.04 ± 0.02	0.1 ± 0.05	0.03 ± 0.11	0.03 ± 0.038
contrac	1473	8	1	0.707 ± 0.04	0.735 ± 0.01	0.684 ± 0.04	0.751 ± 0.14	0.703 ± 0.028
credit_approval	690	10	5	0.23 ± 0.02	0.22 ± 0.01	0.23 ± 0.04	0.26 ± 0.15	0.23 ± 0.01
dermatology	366	34	0	0.02 ± 0.04	0.02 ± 0.02	0.03 ± 0.05	0.04 ± 0.15	0.03 ± 0.01
ecoli	336	7	0	0.17 ± 0.05	0.19 ± 0.02	0.19 ± 0.03	0.17 ± 0.07	0.19 ± 0.02
flags	194	22	6	0.43 ± 0.04	0.42 ± 0.05	0.43 ± 0.06	0.54 ± 0.14	0.42 ± 0.02
glass	214	9	0	0.36 ± 0.05	0.33 ± 0.03	0.35 ± 0.05	0.44 ± 0.2	0.32 ± 0.01

haberman_survival	306	3	0	0.37 ± 0.04	0.39 ± 0.03	0.37 ± 0.06	0.43 ± 0.2	0.46 ± 0.12
hayes_roth	132	0	4	0.32 ± 0.08	0.32 ± 0.03	0.36 ± 0.03	0.34 ± 0.2	0.32 ± 0.1
heart_cleveland	303	10	3	0.53 ± 0.11	0.52 ± 0.07	0.53 ± 0.03	0.49 ± 0.2	0.51 ± 0.08
heart_hungarian	294	10	3	0.11 ± 0.12	0.13 ± 0.08	0.13 ± 0.2	0.19 ± 0.2	0.15 ± 0.17
heart_switzerland	123	10	3	1.05 ± 0.09	0.99 ± 0.09	1.05 ± 0.2	0.98 ± 0.15	0.97 ± 0.23
heart_va	200	10	3	0.87 ± 0.12	0.87 ± 0.11	0.85 ± 0.4	0.83 ± 0.28	0.81 ± 0.023
hepatitis	155	19	0	0.56 ± 0.03	0.58 ± 0.09	0.63 ± 0.2	0.62 ± 0.24	0.46 ± 0.032
hill_valley	606	100	0	0 ± 0.06	0.88 ± 0.12	0.78 ± 0.3	0.12 ± 0.15	0 ± 0.035
hill_valley-noise	606	100	0	0.1 ± 0.02	0.97 ± 0.13	0.94 ± 0.0067	0.35 ± 0.3	0.1 ± 0.039
horse_colic	300	17	4	0.24 ± 0.02	0.26 ± 0.1	0.2 ± 0.0087	0.23 ± 0.1	0.25 ± 0.039
ilpd_indian-liver	583	10	0	0.4 ± 0.02	0.41 ± 0.15	0.4 ± 0.0054	0.38 ± 0.09	0.38 ± 0.02
image_segmentation	210	19	0	0.07 ± 0.5	0.08 ± 0.12	0.09 ± 0.0049	0.13 ± 0.17	0.07 ± 0.02
ionosphere	351	34	0	0.15 ± 0.4	0.18 ± 0.07	0.19 ± 0.0095	0.12 ± 0.17	0.14 ± 0.02
iris	150	4	0	0.09 ± 0.7	0.06 ± 0.07	0.08 ± 0.04	0.06 ± 0.07	0.03 ± 0.06
led_display	1000	7	0	0.318 ± 0.2	0.314 ± 0.04	0.305 ± 0.03	0.321 ± 0.03	0.319 ± 0.03
lenses	24	4	0	0.5 ± 0.7	0.6 ± 0.07	0.4 ± 0.03	0.7 ± 0.08	0.6 ± 0.01
letter	20000	16	0	0.0315 ± 0.002	0.0363 ± 0.08	0.0368 ± 0.03	0.0476 ± 0.11	0.0234 ± 0.01
libras	360	90	0	0.15 ± 0.003	0.2 ± 0.16	0.24 ± 0.04	0.16 ± 0.05	0.1 ± 0.009
low_res-spect	531	100	1	0.41 ± 0.003	0.49 ± 0.16	0.52 ± 0.04	0.52 ± 0.07	0.35 ± 0.009
lung_cancer	32	13	43	0.8 ± 0.009	0.6 ± 0.17	0.7 ± 0.12	0.8 ± 0.1	0.9 ± 0.009
magic	19020	10	0	0.1735 ± 0.002	0.1852 ± 0.15	0.1765 ± 0.04	0.2045 ± 0.2	0.179 ± 0.007
mammographic	961	3	2	0.31 ± 0.02	0.31 ± 0.14	0.31 ± 0.08	0.43 ± 0	0.39 ± 0.005
molec_biol-promoter	106	0	57	0.6 ± 0.02	0.64 ± 0.04	0.68 ± 0.15	0.85 ± 0.1	0.81 ± 0.006
molec_biol-splice	3190	0	60	0.07 ± 0.02	0.068 ± 0.04	0.058 ± 0.015	0.311 ± 0.2	0.069 ± 0.007
monks_1	124	2	4	0.02 ± 0.02	0.02 ± 0.03	0.18 ± 0.015	0.3 ± 0.005	0.19 ± 0.007
monks_2	169	2	4	0.63 ± 0.03	0.63 ± 0.01	0.55 ± 0.011	0.7 ± 0.012	0.36 ± 0.05
monks_3	122	2	4	0.14 ± 0.05	0.14 ± 0.03	0.19 ± 0.013	0.13 ± 0.009	0.18 ± 0.05
mushroom	8124	7	15	0 ± 0.06	0 ± 0.07	0.002 ± 0.016	0.001 ± 0.003	0 ± 0.03
musk_1	476	166	0	0.2 ± 0.02	0.21 ± 0.06	0.2 ± 0.03	0.21 ± 0.007	0.19 ± 0.04
musk_2	6598	166	0	0.026 ± 0.08	0.027 ± 0.08	0.018 ± 0.04	0.049 ± 0.07	0.023 ± 0.03
nursery	12960	6	2	$3e - 04 \pm 0.03$	0.0029 ± 0.06	$9e - 04 \pm 0.06$	0.038 ± 0.09	$5e - 04 \pm 0.11$
optical	3823	64	0	0.019 ± 0.03	0.021 ± 0.07	0.022 ± 0.12	0.023 ± 0.08	0.013 ± 0.1

ozone	2534	72	0	0.06 ± 0.04	0.059 ± 0.14	0.056 ± 0.09	0.061 ± 0.08	0.057 ± 0.08
page_blocks	5473	10	0	0.027 ± 0.04	0.028 ± 0.09	0.027 ± 0.11	0.031 ± 0.06	0.026 ± 0.09
parkinsons	195	22	0	0.31 ± 0.04	0.25 ± 0.14	0.33 ± 0.1	0.33 ± 0.01	0.21 ± 0.04
pendigits	7494	16	0	0.005 ± 0.04	0.009 ± 0.21	0.009 ± 0.12	0.007 ± 0.015	0.004 ± 0.005
pima	768	8	0	0.34 ± 0.03	0.36 ± 0.2	0.37 ± 0.07	0.35 ± 0.012	0.37 ± 0.005
pittsburgh_bridges-MATERIAL	106	4	3	0.45 ± 0.02	0.45 ± 0.09	0.49 ± 0.06	0.88 ± 0.02	0.59 ± 0.003
pittsburgh_bridges-REL-L	103	4	3	0.42 ± 0.03	0.42 ± 0.14	0.41 ± 0.1	0.48 ± 0.01	0.46 ± 0.02
pittsburgh_bridges-SPAN	92	4	3	0.6 ± 0.03	0.6 ± 0.11	0.6 ± 0.1	0.6 ± 0.03	0.5 ± 0.007
pittsburgh_bridges-T-OR-D	102	4	3	0.93 ± 0.04	0.93 ± 0.12	0.67 ± 0.07	0.93 ± 0.04	0.8 ± 0.013
pittsburgh_bridges-TYPE	106	4	3	0.61 ± 0.06	0.63 ± 0.1	0.73 ± 0.1	0.89 ± 0.04	0.65 ± 0.016
planning	182	12	0	0.4 ± 0.07	0.4 ± 0.15	0.52 ± 0.08	0.38 ± 0.03	0.42 ± 0.01
post_operative	90	8	0	0.4 ± 0.05	0.5 ± 0.33	0.4 ± 0	0.5 ± 0.06	0.5 ± 0.009
ringnorm	7400	20	0	0.039 ± 0.05	0.079 ± 0.16	0.037 ± 0	0.041 ± 0.016	0.044 ± 0.011
seeds	210	7	0	0.09 ± 0.05	0.1 ± 0.15	0.11 ± 0.002	0.12 ± 0.014	0.09 ± 0.012
semeion	1593	256	0	0.066 ± 0.005	0.063 ± 0.21	0.063 ± 0.001	0.09 ± 0.011	0.056 ± 0.012
soybean	307	22	13	0.1 ± 0.017	0.1 ± 0.01	0.1 ± 0	0.1 ± 0.011	0.09 ± 0.017
spambase	4601	57	0	0.071 ± 0.009	0.078 ± 0.05	0.074 ± 0.05	0.096 ± 0.011	0.066 ± 0.008
spect	80	22	0	0.7 ± 0.031	0.6 ± 0.09	0.6 ± 0.09	0.6 ± 0.3	0.7 ± 0.012
spectf	80	44	0	0.4 ± 0.008	0.5 ± 0.04	0.6 ± 0.07	0.4 ± 0.2	0.5 ± 0.07
statlog_australian-credit	690	10	4	0.23 ± 0.011	0.22 ± 0	0.24 ± 0.05	0.28 ± 0.3	0.25 ± 0.08
statlog_german-credit	1000	14	6	0.336 ± 0.013	0.35 ± 0.06	0.364 ± 0.06	0.384 ± 0.3	0.346 ± 0.04
statlog_heart	270	10	3	0.32 ± 0.011	0.3 ± 0.13	0.29 ± 0.007	0.31 ± 0.3	0.35 ± 0.04
statlog_image	2310	19	0	0.02 ± 0.018	0.023 ± 0.07	0.017 ± 0.008	0.035 ± 0.2	0.017 ± 0.04
statlog_landsat	4435	36	0	0.115 ± 0.023	0.117 ± 0.05	0.108 ± 0.005	0.122 ± 0.2	0.108 ± 0.067
statlog_shuttle	43500	9	0	$2e - 04 \pm 0.011$	$3e - 04 \pm 0.05$	$3e - 04 \pm 0.01$	0.0013 ± 0.1	$3e - 04 \pm 0.076$
statlog_vehicle	846	18	0	0.26 ± 0.014	0.32 ± 0.07	0.31 ± 0.01	0.31 ± 0.1	0.22 ± 0.065
steel_plates	1941	27	0	0.319 ± 0.009	0.306 ± 0.08	$0.289 \pm 5e - 04$	0.356 ± 0.3	0.336 ± 0.058
synthetic_control	600	60	0	0.02 ± 0.018	0.01 ± 0.02	0.02 ± 0.0012	0.02 ± 0.04	0.01 ± 0.059
teaching	151	3	2	0.61 ± 0.016	0.64 ± 0.07	0.7 ± 0.0011	0.61 ± 0.04	0.57 ± 0.048
thyroid	3772	21	0	0.032 ± 0.0041	0.028 ± 0.06	0.035 ± 0.0018	0.616 ± 0.06	0.053 ± 0.037
tic_tac-toe	958	0	9	0.04 ± 0.0041	0.03 ± 0.05	$0.03 \pm 7e - 04$	0.45 ± 0.03	0.05 ± 0.027
titanic	2201	2	1	0.309 ± 0.0079	0.309 ± 0.04	0.315 ± 0.005	0.315 ± 0.02	0.315 ± 0.048

twonorm	7400	20	0	0.045 ± 0.0028	0.052 ± 0.01	0.051 ± 0.006	0.043 ± 0.035	0.045 ± 0.038
vertebral_column_task_1	310	6	0	0.22 ± 0.0047	0.25 ± 0.06	0.28 ± 0.006	0.22 ± 0.037	0.24 ± 0.043
vertebral_column_task_2	310	6	0	0.32 ± 0.004	0.34 ± 0.01	0.34 ± 0.004	0.37 ± 0.065	0.31 ± 0.057
wall_following	5456	24	0	0.007 ± 0.005	0.007 ± 0.07	0.004 ± 0.004	0.166 ± 0.039	0.037 ± 0.054
waveform	5000	21	0	0.205 ± 0.006	0.221 ± 0.07	0.208 ± 0.006	0.205 ± 0.019	0.209 ± 0.042
waveform_noise	5000	40	0	0.201 ± 0.013	0.211 ± 0.05	0.208 ± 0.008	0.21 ± 0.03	0.197 ± 0.054
wine	178	13	0	0.05 ± 0.004	0.06 ± 0.06	0.03 ± 0.008	0.04 ± 0.05	0.03 ± 0.08
wine_quality-red	1599	11	0	0.527 ± 0.04	0.538 ± 0.05	0.548 ± 0.003	0.529 ± 0.1	0.523 ± 0.06
wine_quality-white	4898	11	0	0.562 ± 0.04	0.572 ± 0.05	0.58 ± 0.005	0.566 ± 0.06	0.57 ± 0.05
yeast	1484	8	0	0.523 ± 0.03	0.52 ± 0.04	0.528 ± 0.005	0.535 ± 0.02	0.538 ± 0.06
zoo	101	16	0	0.07 ± 0.02	0.06 ± 0.02	0.07 ± 0.003	0.06 ± 0.011	0.06 ± 0.08

Table 2: Five-fold cross-validation error rates (mean \pm SEM) on the UCI datasets, along with summary statistics for each dataset. n is the number of examples, p_{num} is the number of numeric features, and p_{cat} is the number of categorical features.

Dataset	n	p_{num}	p_{cat}	5-fold CV Error Rate		
				Lumberjack	RF	CCF
auto_price	158	16	0	13.55 ± 10.44	13.45 ± 9.68	10.91 ± 7.57
auto93	92	20	3	37.18 ± 29.56	38.06 ± 33.10	27.31 ± 32.94
autoHorse	202	18	8	11.98 ± 11.97	13.77 ± 13.73	10.89 ± 14.89
autoMpg	397	7	1	26.48 ± 2.69	12.72 ± 2.51	11.53 ± 4.56
basketball	95	5	0	73.41 ± 32.65	78.37 ± 40.26	72.77 ± 31.73
bodyfat	251	15	0	3.25 ± 2.24	7.35 ± 3.83	4.73 ± 3.26
bolts	39	8	0	10.20 ± 3.93	14.02 ± 4.69	8.62 ± 8.05
breastTumor	285	4	6	108.10 ± 21.76	101.37 ± 16.29	108.1 ± 25.03
cholesterol	302	11	3	111.76 ± 30.52	102.34 ± 27.24	99.71 ± 43.48
cleveland	302	11	3	59.76 ± 19.08	50.70 ± 13.73	48.15 ± 14.20
cloud	107	5	2	21.80 ± 14.45	19.37 ± 17.05	22.09 ± 22.59
cpu	208	7	1	7.06 ± 10.54	8.76 ± 13.26	8.07 ± 20.08
detroit	12	14	0	35.04 ± 45.21	30.41 ± 39.55	39.20 ± 78.01
diabetes_numeric	42	3	0	69.52 ± 26.07	64.86 ± 30.09	70.84 ± 45.65
echoMonths	129	10	0	54.47 ± 9.96	52.48 ± 10.33	56.94 ± 19.42
elusage	54	3	0	21.61 ± 2.39	22.43 ± 6.77	21.29 ± 13.25
fishcatch	157	7	1	3.87 ± 1.69	4.73 ± 2.60	2.17 ± 2.35
fruitfly	124	4	1	136.57 ± 67.04	132.26 ± 75.55	128.6 ± 66.66
gascons	26	5	0	9.13 ± 8.16	11.41 ± 9.73	4.02 ± 4.68
housing	505	14	0	12.05 ± 4.46	12.01 ± 3.38	12.89 ± 8.47
hungarian	293	11	3	61.40 ± 12.02	55.57 ± 11.92	50.94 ± 14.55
longley	15	7	0	14.15 ± 8.36	12.67 ± 7.88	6.61 ± 7.56
lowbwt	188	9	1	46.23 ± 13.90	39.67 ± 8.42	40.09 ± 13.68
machine_cpu	208	7	0	13.50 ± 8.62	11.24 ± 8.51	12.80 ± 23.68
mbagrade	60	3	0	125.95 ± 48.45	129.32 ± 49.15	106.1 ± 69.36
meta	527	20	2	92.90 ± 105.28	88.68 ± 110.79	93.29 ± 159.3
pbcc	417	18	1	110.18 ± 25.72	64.09 ± 8.11	62.81 ± 12.95
pharynx	194	11	2	38.53 ± 14.60	43.11 ± 19.58	36.25 ± 16.41
pollution	59	16	0	44.87 ± 26.43	46.83 ± 28.24	43.35 ± 30.47
pwLinear	199	11	0	14.19 ± 1.50	19.00 ± 1.98	15.33 ± 5.61
pyrim	73	28	0	61.65 ± 79.80	62.51 ± 88.43	58.21 ± 113.2
quake	2177	4	0	107.60 ± 7.97	107.68 ± 8.97	106.1 ± 11.97
schlvote	36	6	0	72.11 ± 122.22	77.30 ± 127.48	78.31 ± 141.5
sensory	575	12	0	77.31 ± 10.55	76.98 ± 10.52	77.27 ± 12.74
servo	166	1	4	33.07 ± 13.20	17.80 ± 22.41	10.93 ± 14.87
sleep	57	8	0	57.23 ± 22.26	61.83 ± 22.47	48.24 ± 23.37
stock	949	10	0	1.16 ± 0.21	1.37 ± 0.31	1.11 ± 0.22
strike	624	6	1	89.32 ± 76.93	86.39 ± 77.94	87.35 ± 100.0
triazines	185	61	0	61.97 ± 13.69	70.02 ± 14.50	71.99 ± 36.69
veteran	136	7	1	103.06 ± 44.63	86.39 ± 55.73	80.39 ± 77.45
vineyard	51	4	0	33.20 ± 26.14	31.74 ± 24.73	34.86 ± 27.98
wisconsin	193	33	0	90.17 ± 11.11	93.75 ± 9.83	87.82 ± 24.18

Table 3: Five-fold cross-validation error rates (mean \pm SEM) on 42 of the 62 regression WEKA datasets, along with summary statistics for each dataset. n is the number of examples, p_{num} is the number of numeric features, and p_{cat} is the number of categorical features.

References

- Dimitris Achlioptas. Database-friendly random projections: Johnson-lindenstrauss with binary coins. *Journal of computer and System Sciences*, 66(4):671–687, 2003.
- G. Biau, L. Devroye, and G. Lugosi. Consistency of random forests and other averaging classifiers. *The Journal of Machine Learning Research*, 9:2015–2033, 2008.
- G rard Biau, Erwan Scornet, and Johannes Welbl. Neural random forests. *arXiv preprint arXiv:1604.07143*, 2016.
- Ella Bingham and Heikki Mannila. Random projection in dimensionality reduction: applications to image and text data. In *Proceedings of the seventh ACM SIGKDD international conference on Knowledge discovery and data mining*, pages 245–250. ACM, 2001.
- Rico Blaser and Piotr Fryzlewicz. Random rotation ensembles. *Journal of Machine Learning Research*, 17(4):1–26, 2016.
- Leo Breiman et al. Arcing classifier (with discussion and a rejoinder by the author). *The annals of statistics*, 26(3):801–849, 1998.
- L. Breiman. Random forests. *Machine Learning*, 4(1):5–32, October 2001.
- James Browne, Tyler Tomita, and Joshua T. Vogelstein. *ref: Randomer Forest*, 2018.
- James Browne, Tyler M Tomita, Disa Mhembere, Randal Burns, and Joshua T Vogelstein. Forest packing: Fast, parallel decision forests. June 2018.
- Rich Caruana and Alexandru Niculescu-Mizil. An empirical comparison of supervised learning algorithms. In *Proceedings of the 23rd international conference on Machine learning*, pages 161–168. ACM, 2006.
- R. Caruana, N. Karampatziakis, and A. Yessenalina. An empirical evaluation of supervised learning in high dimensions. *Proceedings of the 25th International Conference on Machine Learning*, 2008.
- Tianqi Chen and Carlos Guestrin. Xgboost: A scalable tree boosting system. In *Proceedings of the 22nd acm sigkdd international conference on knowledge discovery and data mining*, pages 785–794. ACM, 2016.
- Tianqi Chen. *xgboost: Extreme Gradient Boosting*, 2018.
- Sanjoy Dasgupta and Yoav Freund. Random projection trees and low dimensional manifolds. In *Proceedings of the Fortieth Annual ACM Symposium on Theory of Computing*, STOC '08, pages 537–546, New York, NY, USA, 2008. ACM.
- S Dasgupta and Y Freund. Random projection trees for vector quantization. *IEEE Transactions on Information*, 2009.
- S Dasgupta and K Sinha. Randomized partition trees for exact nearest neighbor search. *Conference on Learning Theory*, 2013.

- L. Devroye, L. Györfi, and G. Lugosi. *A Probabilistic Theory of Pattern Recognition*. 1996.
- Dirk Eddebuettel. *Rcpp: Seamless R and C++ Integration*, 2018.
- Xiaoli Z Fern and Carla E Brodley. Random projection for high dimensional data clustering: A cluster ensemble approach. In *Proceedings of the 20th international conference on machine learning (ICML-03)*, pages 186–193, 2003.
- M. Fernandez-Delgado, E. Cernadas, S. Barro, and D. Amorim. Do we need hundreds of classifiers to solve real world classification problems? *Journal of Machine Learning Research*, 15(1):3133–3181, October 2014.
- Dmitriy Fradkin and David Madigan. Experiments with random projections for machine learning. In *Proceedings of the ninth ACM SIGKDD international conference on Knowledge discovery and data mining*, pages 517–522. ACM, 2003.
- Jerome H Friedman. Greedy function approximation: a gradient boosting machine. *Annals of statistics*, pages 1189–1232, 2001.
- D. Heath, S. Kasif, and S. Salzberg. Induction of oblique decision trees. *Journal of Artificial Intelligence Research*, 2(2):1–32, 1993.
- Chinmay Hegde, Michael Wakin, and Richard Baraniuk. Random projections for manifold learning. In *Advances in neural information processing systems*, pages 641–648, 2008.
- Gareth M James. Variance and bias for general loss functions. *Machine Learning*, 51(2):115–135, 2003.
- Guolin Ke, Qi Meng, Thomas Finley, Taifeng Wang, Wei Chen, Weidong Ma, Qiwei Ye, and Tie-Yan Liu. Lightgbm: A highly efficient gradient boosting decision tree. In I. Guyon, U. V. Luxburg, S. Bengio, H. Wallach, R. Fergus, S. Vishwanathan, and R. Garnett, editors, *Advances in Neural Information Processing Systems 30*, pages 3146–3154. Curran Associates, Inc., 2017.
- Yann Lecun, Corinna Cortes, and Christopher J.C. Burges. *The MNIST Database of Handwritten Digits*.
- P. Li, T. J. Hastie, and K. W. Church. Very sparse random projections. In *Proceedings of the 12th ACM SIGKDD international conference on Knowledge discovery and data mining*, pages 287–296. ACM, 2006.
- Gilles Louppe. Understanding random forests: From theory to practice. *arXiv preprint arXiv:1407.7502*, 2014.
- Nicolai Meinshausen. Quantile regression forests. *J. Mach. Learn. Res.*, 7(Jun):983–999, 2006.
- B. H. Menze, B.M Kelm, D. N. Splitthoff, U. Koethe, and F. A. Hamprecht. On oblique random forests. In Dimitrios Gunopulos, Thomas Hofmann, Donato Malerba, and Michalis Vazirgiannis, editors, *Machine Learning and Knowledge Discovery in Databases*, volume 6912 of *Lecture Notes in Computer Science*, pages 453–469. Springer Berlin Heidelberg, 2011.

- Tom Rainforth and Frank Wood. Canonical correlation forests. *arXiv preprint arXiv:1507.05444*, 2015.
- J. J. Rodriguez, L. I. Kuncheva, and C. J. Alonso. Rotation forest: A new classifier ensemble method. *Pattern Analysis and Machine Intelligence, IEEE Transactions on*, 28(10):1619–1630, 2006.
- Robert E Schapire. The strength of weak learnability. *Mach. Learn.*, 5(2):197–227, July 1990.
- Charles J Stone. Consistent nonparametric regression. *The annals of statistics*, pages 595–620, 1977.
- Tyler M Tomita, Mauro Maggioni, and Joshua T Vogelstein. Roflmao: Robust oblique forests with linear matrix operations. In *SIAM Data Mining*, 2017.
- G. V. Trunk. A problem of dimensionality: A simple example. *Pattern Analysis and Machine Intelligence, IEEE Transactions on*, (3):306–307, 1979.
- Roman Vershynin. *High Dimensional Probability: An Introduction with Applications in Data Science*. 2017.
- Marvin N. Wright. *ranger: A fast Implementation of Random Forests*, 2018.
- A J Wyner, M Olson, J Bleich, and D Mease. Explaining the success of adaboost and random forests as interpolating classifiers. *J. Mach. Learn. Res.*, 2017.
- Laurent Younes. Diffeomorphic Learning. *arXiv preprint arXiv:1806.01240*, 2018.